https://doi.org/10.5194/egusphere-2026-2593
Preprint. Discussion started: 23 June 2026

Measurement report: Size-resolved seasonal study of inorganic ions and isotopic carbon signatures of aerosol particles at the Wadden Sea

Katrin Zenker[1], Peter Redl[2,*], Anne Kasper-Giebl[2], and Ulrike Dusek[1]

[1]Centre for Isotope Research, University of Groningen, The Netherlands
[2]Division Environmental Analytics, Institute of Chemical Technologies and Analytics, Vienna University of Technology, Austria
[*]now working at: GeoSphere Austria, Chemical Weather Forecasts, Vienna, Austria

Correspondence: Ulrike Dusek (u.dusek@rug.nl)

Abstract. Measurements of aerosol size-resolved chemical composition and source contribution of carbonaceous aerosols provide a unique opportunity to characterize continental outflow over the sea. Studies at coastal sites usually show an interesting mix of continental and marine aerosol sources. However, few data exist on the size dependence of the aerosol chemical composition and isotopic source apportionment of organic carbon (OC). This study aims to quantify seasonal, air-mass, and size-dependent variations in inorganic aerosol composition and OC sources. It also highlights isotope measurements as a tool to study sources and atmospheric processing of OC. Size-resolved measurements of inorganic ions, levoglucosan, and total carbon (TC) were combined with ^{13}C and ^{14}C analysis of OC at different desorption temperatures, which allows to investigate subgroups like secondary organic aerosol (SOA) and aged organic aerosol. During continental outflow conditions, nitrate, ammonium, and TC dominated, while sulfate and TC dominated under marine influence. Sulfate reached up to 0.5 µg/m^3 both in marine and regional continental air, indicating the importance of ship emissions. Fossil OC fractions were highest in particles <250 nm, characteristic for traffic emissions. $^{13}C/^{12}C$-ratios of ambient OC deviate strongly from expected signatures of primary sources and indicate SOA contribution to more volatile carbon and smaller particles. The $^{13}C/^{12}C$-ratios of less volatile OC at larger sizes are consistent with a significant influence of photochemical processing. The results highlight shipping emissions as the main source of sulfate aerosols at this coastal site and demonstrate the highly processed nature of OC in the European continental outflow.

1 Introduction

Particulate matter (PM) has a significant impact on human health (e.g. Nel, 2005; Pope III and Dockery, 2006) and the global climate (e.g. Boucher et al., 2013; Myhre et al., 2013), due to scattering and absorption of solar radiation. The full extent of this influence is still not yet completely understood, but it is certain, that the size of the airborne particles and their chemical composition play an important role. The size of the particles determines, whether and where particles are deposited in the lung and whether they can enter the blood stream (Pöschl, 2005). Scattering or absorption coefficients of ambient aerosol particles, also depend crucially on their size and chemical composition.

https://doi.org/10.5194/egusphere-2026-2593
Preprint. Discussion started: 23 June 2026

The size and chemical composition of aerosol particles depend on their sources and on transformation processes in the atmosphere. In order to improve e.g. climate models and allow policy makers to develop mitigation strategies for a better air quality, the knowledge about the sources and transformation mechanism of aerosols needs to be improved.

Previous studies showed that in the Netherlands the aerosol chemical composition is dominated by secondary inorganic aerosol (Weijers et al., 2011), which is the sum of sulfate, nitrate and ammonium. The second largest contribution is from carbonaceous constituents and the most important natural source is sea salt.

In general, in Europe the carbonaceous aerosol fraction takes up 30 % to 60 % of PM2.5, i.e. particulate matter with an aerodynamic diameter of smaller than 2.5 µm (e.g. Pöschl, 2005; Fuzzi et al., 2015; Putaud et al., 2004). The total carbon (TC) content of aerosol is usually operationally divided into organic carbon (OC) and elemental carbon (EC) (TC=OC+EC). EC is produced from primary sources during incomplete combustion and is in general inert in the atmosphere. OC is also directly emitted by incomplete combustion and other processes, like cooking, or biogenic activity in the form of e.g. pollen fragments. In addition to these primary sources, secondary organic carbon (SOC) is formed from the oxidation of precursor gases and condenses on pre-existing particles. Contrary to elemental carbon, OC is not inert and its chemical composition is continuously changed by transformation mechanisms in the atmosphere.

Analysis of the carbon isotopes ^{13}C and ^{14}C can give insights into sources and atmospheric chemistry of carbonaceous aerosols (e.g. Szidat et al., 2006; Dusek et al., 2017; Masalaite et al., 2020; Ni et al., 2022). Since ^{14}C has decayed in fossil fuels (Schuur et al., 2016), but is present at a typical contemporary $^{14}C/^{12}C$ ratio in living biomass, it allows to apportion fossil (^{14}C free) or non-fossil carbon sources for carbonaceous aerosols. The radiocarbon isotopic composition of organic aerosol is not significantly influenced by atmospheric transformation processes. The $^{13}C/^{12}C$-ratios of EC and OC also gives an insight into aerosol sources, e.g. enabling to distinguish between C3 and C4 plant types of sources (O'Leary, 1988; Vernooij et al., 2022), but in many regions, including Western Europe, ^{13}C alone is not suitable for source apportionment, because the different source signatures are overlapping (e.g. Martinsson et al., 2017). Nonetheless, the measurement of the ^{13}C isotopic signature of organic aerosol facilitates the characterisation of atmospheric transformation mechanism, as $^{13}C/^{12}C$ ratios are changed by chemical reactions (e.g. Kirillova et al., 2013; Gensch et al., 2014; Huang et al., 2006).

During the formation of secondary organic aerosol (SOA) from precursor volatile organic carbon (VOC), ^{12}C reacts preferentially due to the kinetic isotope effect. The reaction products are therefore expected to be depleted in ^{13}C compared to the precursor gas, if it is not completely consumed. In this case, the $^{13}C/^{12}C$ ratio in the SOA will be less than in the precursor gas (and usually also the primary OA) and the condensing SOA gradually leads to lower $^{13}C/^{12}C$ ratio of the overall OC. Since condensing organic vapors will contribute relatively more mass to smaller particle, this effect should be more noticeable at smaller particle sizes.

In the presented study the ^{13}C of organic carbonaceous aerosol was analyzed at three different temperature steps (200 °C, 350 °C, 650 °C), which reflect different volatility fractions of OC-species (Zenker et al., 2020). More volatile OC, associated with freshly emitted primary fossil fuel burning aerosol or newly formed SOA, tends to be evolved from the filter at lower temperature and more thermally stable OC desorbs at higher temperature (Masalaite et al., 2018; Holzinger et al., 2013). Higher thermal stability of organic carbon is often observed after the aerosol is transformed by photochemical or aqueous-phase

https://doi.org/10.5194/egusphere-2026-2593
Preprint. Discussion started: 23 June 2026

processes (Masalaite et al., 2017; Ni et al., 2022). These processes, also known as aerosol aging, result in more oxidized and therefore more thermally stable aerosol (Donahue et al., 2009; Holzinger et al., 2013). Considering the particle size distribution, primary anthropogenic combustion sources emit preferentially smaller particles ($D_{50} < 0.18\,\mu m$; Masalaite et al., 2018). On the other hand, aerosol aging is more relevant for larger particles, in the size range of accumulation mode, due to their longer residence time in the atmosphere, which gives transformation processes more time to alter the aerosol. Local combustion sources are therefore primarily reflected in the composition of the smaller primary aerosol particles. Sources further away are associated with the long range transport of aerosol, and are therefore displayed at larger particle sizes, which are additionally affected by aging processes.

For the process of photochemical aging it is postulated (e.g. Ni et al., 2022; Masalaite et al., 2020), that OC in the particle becomes gradually enriched in ^{13}C compared to the original particle composition. This is caused by the gradual volatilization of OC, which proceeds faster for ^{12}C containing compounds, because molecular bonds involving ^{12}C are more easily broken. This results in a net loss of the isotopically lighter carbon ^{12}C in the particle. If the particle is only partially oxidized, the remaining OC in the particle is enriched in ^{13}C compared to OC of the original particle.

This study presents results for the mass concentrations of inorganic ions and total carbon, and the carbon isotope ratios $^{13}C/^{12}C$ and $^{14}C/^{12}C$ of organic carbon for size-resolved fine aerosol particles. While bulk chemical composition is measured routinely at many European sites, size resolved chemical composition data are much more rare, especially combined with isotope source apportionment of the organic aerosol. This allows more detailed insights into the inorganic and organic chemistry of various size aerosol fractions and related atmospheric transformation mechanisms. Results are based on a long term sampling campaign, which makes it possible to investigate seasonal variations. The special set-up of the sampling campaign allows to investigate aerosol from the North Sea and aerosol, that is originating from the land and advecting to the sea. This aerosol can probably change the radiation budget of the sea surface as the particle absorb or reflect light. The sampling location very close to the sea is in general of significance, as many aerosol studies are available for continental and urban sites, but much less data exist for coastal sites (Chesselet et al., 1981; Ceburnis et al., 2011; Turšič et al., 2006).

2 Methods

2.1 Sampling and filter handling

A sampling campaign was conducted during 2015/16 to collect size-resolved aerosol samples at the Lutjewad atmospheric measurement station located directly behind the dyke at the Wadden Sea in the Netherlands. The sampling equipment has been set up on a scaffold at about 10.5 m, which is higher than the dyke (see figure A1). The sampling equipment consisted of a custom-made setup with two impactors (MSP-model 130-HFI) and a weather station.

The impactor setup is shown in figure 1. The two impactors are connected to the sampling pump via two controllable solenoid 3-way valves. At any given time either one of the impactors is sampling or the air is flowing through a bypass directly to the pump. The setting of the valves is controlled by a customised LabVIEW program, so that each impactor samples only from

https://doi.org/10.5194/egusphere-2026-2593
Preprint. Discussion started: 23 June 2026

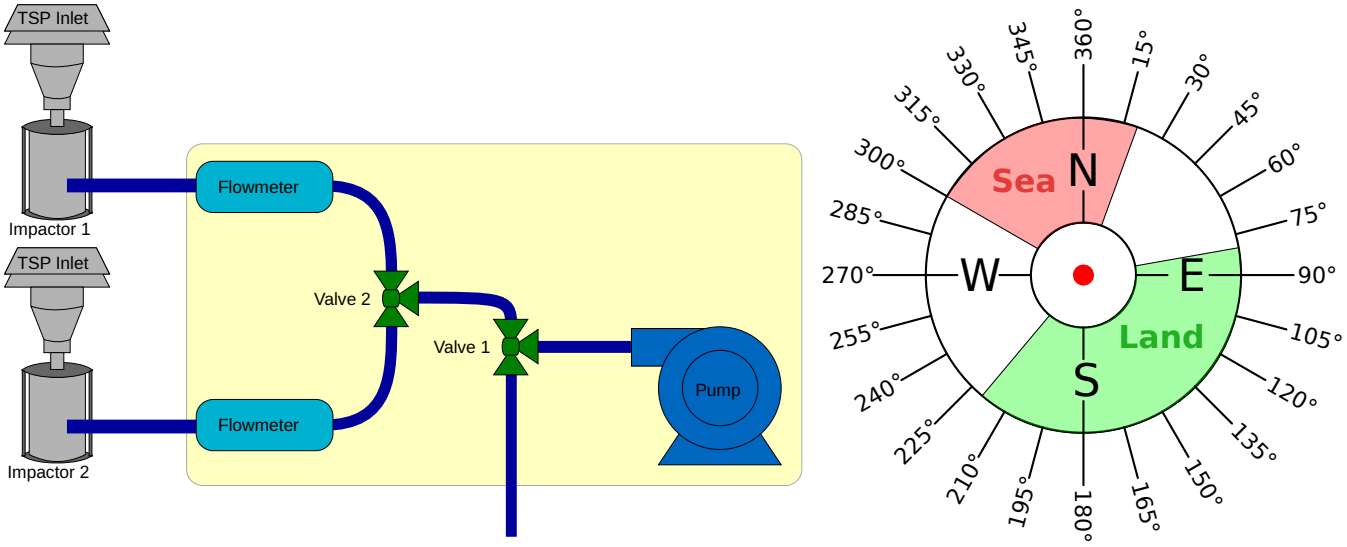

Figure 1. Sampling Setup: An outline of the wind direction selective sampling setup with two impactors is shown on the left. The impactors are equipped with a TSP (total suspended particulates) inlet. The flow meters, valves and the pump are in a weather-proof housing (yellow box). The right indicates an example of wind sectors for impactor 1 and 2, e.g. impactor 1 would collect aerosol particles only from 'Land' wind directions, impactor 2 only from 'Sea' wind directions. If the wind comes from neither sector, the pump samples from the bypass via valve 1.

a given (custom-defined) wind sector. If air is coming from outside the wind sectors, neither impactor is sampling. Sampling will also only start when the wind velocity is above 2 m/s to avoid baffling wind.

The location directly at the Wadden Sea made it possible to collect aerosol from a 'land' sector (E - SSW) on one impactor and aerosol from the 'sea' sector (WSW - NE) on the other. The land sector is mostly influenced by sources in continental Europe including possible transformation processes during long-range transport. This type of aerosol is of special interest, as it will be advected in the direction of the ocean and influence the radiative forcing over the North Sea (Jayaraman et al., 1998). On the other hand the air from the sea sector is likely much cleaner (Fitzgerald, 1991; Ceburnis et al., 2011) and is mainly influenced by marine aerosol or regional sources, e.g. ship emissions from the highly frequented English Channel (Matthias et al., 2010). In addition 72-hour back-trajectories were calculated using the HYSPLIT trajectory model (Stein et al., 2015; Rolph et al., 2017) (see figure 3 and figure C1) for the sampling periods of each impactor.

The high flow cascade impactor had an inlet flow rate of 100 l/min and consists of five stages and a back-up filter. It allows sampling in the following aerodynamic particle size ranges: 1.4 - 2.5 µm, 0.77 - 1.4 µm, 0.44 - 0.77 µm, 0.25 - 0.44 µm, 0 - 0.25 µm. To convert the measured concentrations to mass size distributions $dM/dlnD_p$, we assume a lower cut-off size of 0.05 µm for the back-up filter, as the contribution of particles below that size to the measured mass is negligible (Ni et al., 2022). In this study quartz fibre filters (75 mm and 90 mm (back-up filter); Pallflex membrane filters, type tissuquartz 2500QUAT-UP) were used as impaction substrates, which required customization of the distance ring for the last two impactor stages. The quartz fibre filters were pre-cleaned at 650 °C for two hours, before using them for sampling. After removing the filters from

https://doi.org/10.5194/egusphere-2026-2593
Preprint. Discussion started: 23 June 2026

Table 1. Overview of filter samples: start and end dates are the times when the impactors are set up, not actually the start or end of sampling

filtername	start	end	sampling time [days]	season	sampled wind direction [°]	sample type
AU15_L2	27.10.15	12.11.15	10.63	autumn	80 - 220	land
WI16_L1	04.02.16	15.02.16	2.25	winter	90 - 185	land
WI16_L2	15.02.16	02.03.16	3.98	winter	90 - 185	land
SP16_L1	06.04.16	19.04.16	2.84	spring	90 - 185	land
SP16_L2	19.04.16	04.05.16	1.72	spring	90 - 185	land
SU16_L3	25.07.16	09.08.16	2.00	summer	90 - 185	land
SU16_L4	09.08.16	24.08.16	2.66	summer	90 - 185	land
SU16_S4	09.08.16	24.08.16	4.62	summer	240 - 30	sea

the impactor, they were wrapped in pre-cleaned (2 h, 550 °C) aluminum foils and stored in sealed polyethylene bags at about -18 °C in the freezer until analysis. Every part of equipment that came into contact with the samples, including impaction plates and tweezers etc., was first cleaned with acetone, then with ethanol and afterwards air-dried.

Table 1 shows the measurement periods (11-18 days) in the different seasons. The sampling time per impactor varied between two and eleven days, depending on time periods with wind from a certain sector. Unfortunately only one sample from the 'sea' wind sector could be analyzed, as the others did not contain enough particle mass.

2.2 Analyses of ions and levoglucosan

Determination of anions (Cl^-, $NO_2{}^-$, $NO_3{}^-$, $SO_4{}^{2-}$), cations (Na^+, $NH_4{}^+$, K^+, Ca^{2+}, Mg^{2+}) and levoglucosan was performed with ion chromatography. For analyses of ions, sample aliquots were extracted with ultrapure water and ultrasonic agitation, followed by centrifugation. Analyses of anions was done with a Dionex ICS1100 system (Thermo Fisher Scientific Inc.) using AS22 and AG22 columns, a self-regenerating suppressor and conductivity detection. The eluent was 4.5 mM Na_2CO_3/1.4 mM $NaHCO_3$, at a flow rate of 1 ml/min. Cations were analysed with a Dionex Aquion system (Thermo Fisher Scientific Inc.) equipped with CS16 and CG16 columns, a self-regenerating suppressor and a conductivity detector. The eluent was 38 mM methanesulfonic acid at an eluent flow of 1 ml/min. Calibration was done with external standards, prepared from Merck stock solutions. Levoglucosan was determined via anion-exchange chromatography and pulsed amperometric detection (HPAE-PAD) with an Dionex ICS3000 system using a CarboPacMA1 as an analytical and a guard column. Gradient elution was done with sodium hydroxide, using concentrations of 480 mM - 650 mM at a flow rate of 0.4 ml/min.

2.3 Measurement of total carbon concentrations

The total carbon concentration of the size-resolved aerosol filter samples was determined with a commercial thermo-optical OC-EC analyzer (Sunset Laboratory Inc., Model 5L). The samples were analyzed with a custom TC protocol, that combusts

https://doi.org/10.5194/egusphere-2026-2593
Preprint. Discussion started: 23 June 2026

the sample in a mixture of helium and 2 % oxygen for 5.5 min at a temperature of 870 °C. The measured total carbon concentrations have been corrected for the instrument blank and the sampling blank. OC/EC analysis was not possible due to the inhomogeneous deposits on the impactor samples.

2.4 Measurement of $\delta(^{13}C)$ signatures

The stable carbon isotope ratio $R(^{13}C/^{12}C)$ of OC in a sample is given in the delta notation, which is defined as follows:

$$\delta(^{13}C/^{12}C, \text{sample/reference}) = \frac{R\left(^{13}C/^{12}C, \text{sample}\right)}{R\left(^{13}C/^{12}C, \text{reference}\right)} - 1 \quad (1)$$

The reference is the international Vienna Pee Dee Belemnite (VPDB) standard and delta values are expressed in ‰. In the following text $\delta(^{13}C)$ is used as the short form of $\delta(^{13}C/^{12}C$, sample/reference).

A detailed description of the setup and the measurement procedure is given in Zenker et al. (2020). Briefly, measurements of $\delta(^{13}C)$ values are conducted with a system that combines a OC-EC analyzer (Sunset Laboratory Inc., Model 5L), where OC is converted to CO_2, with a continuous flow isotope ratio mass spectrometer (IRMS) (Micromass now Isoprime, model Optima). The interface between these two instruments serves to collect, purify and concentrate the extracted CO_2 from the aerosol filter samples. In the Sunset oven the organic carbon is desorbed in helium carrier gas at three different temperature steps (200 °C, 350 °C, 650 °C). The manganese dioxide (MnO_2) catalyst in the Sunset OC-EC analyzer ensures the complete oxidation of the carbon released during the different desorption steps to CO_2.

For the analysis of the coastal filter samples, the system described by Zenker et al. (2020) was updated to include a reduction oven. This oven contains copper and silver to remove traces of oxygen, nitrogen oxides and halogens at a temperature of 600 °C. This treatment was found to significantly improve the repeatability of the filter samples from this coastal location, but is usually not necessary for filters from other locations.

$\delta(^{13}C)$ values were calculated with respect to two reference gas peaks, measured before and after the sample peak. If these two values differ by more than 1 ‰, this certain measurement is rejected from further analysis. $\delta(^{13}C)$ values calculated with respect to the first reference peak are presented in this study. $\delta(^{13}C)$ signatures are calibrated using a two-point linear scale correction based on two different reference materials, which are measured every day. The linear scale correction uses a weekly average of these reference materials and is applied to all samples measured in the respective week. These two in-house reference materials are both caffeines and one of them is enriched in ^{13}C. Their nominal $\delta(^{13}C)$ values are -38.2 ‰ and 0.61 ‰. A third international reference material is analyzed every day and is used for quality control. This internationally agreed upon secondary reference material is L-Valine (Schimmelmann et al., 2016) and has a reference value of -24.03 $\pm$ 0.04 ‰, which is in the range of the expected $\delta(^{13}C)$ values of aerosol particle samples. The average $\delta(^{13}C)$ value of the measured L-Valine reference for a time span of about two years is -24.07 ‰ and the standard deviation amounts to 0.22 ‰. This is an indicator for the precision and the uncertainty of the $\delta(^{13}C)$ values presented in this work.

https://doi.org/10.5194/egusphere-2026-2593
Preprint. Discussion started: 23 June 2026

2.5 Measurement of the fraction modern of carbon ($F(^{14}C)$)

The radiocarbon isotopic composition of an aerosol filter sample is reported as fraction modern ($F(^{14}C)$) according to the nomenclature established by Reimer et al. (2004):

$$F(^{14}C/^{12}C, \text{sample/OxII}) = \frac{R\left(^{14}C/^{12}C, \text{sample}\right)}{0.7459 \cdot R\left(^{14}C/^{12}C, \text{OxII}\right)} \quad (2)$$

Hereby the $^{14}C/^{12}C$ ratio of the sample is given in relation to the ratio of the standard (oxalic acid, OxII). The factor 0.7459 converts the $^{14}C/^{12}C$ ratio of OxII to the value defined by international agreement as representative for an unperturbed atmosphere in the year 1950. The $^{14}C/^{12}C$ ratio of both the sample and the standard are normalized to a $\delta(^{13}C)$ of -25 ‰. In the following text $F(^{14}C)$ is used as the short form of $F(^{14}C/^{12}C$, sample/OxII).

In this study $F(^{14}C)$ of organic carbon is presented. The combustion, extraction and conversion to CO_2 was done using the Automated Aerosol Combustion (AAC) system described in Dusek et al. (2019). Briefly, the aerosol filter sample was combusted in pure oxygen at 375 °C for 8 min. The separation of CO_2 from other interfering gases (e.g. SO_2, NO_x, H_2O or halogens) is done with the help of a reduction oven containing copper and silver, and two water traps. Until analysis the CO_2 is stored in evacuated flame sealed glass tubes.

For radiocarbon measurement the CO_2 is transferred via the gas inlet system to the ion source of the Mini Carbon Dating System (MICADAS). This accelerator mass spectrometer is described in more detail in Synal et al. (2007). The $F(^{14}C)$ values are corrected for the memory effect, the instrument background is subtracted and finally all values are normalized to the average of the oxalic acid (OxII)) gaseous standard, which are analyzed in every batch (Wacker et al., 2010). Furthermore secondary standards are analyzed alongside the unknown samples, which serve as a control of the measurement and data correction (Aerts-Bijma et al., 2021).

To correct for the contamination introduced during combustion in the AAC, small amounts of standard material undergo the same process of combustion and radiocarbon measurement. Here OxII serves for the determination of the fossil contamination and a ^{14}C free background wood standard serves to determine the modern contamination.

3 Results and Discussion

3.1 Chromatographic analysis and total carbon concentrations

Figure 2 shows an overview of the mass size distributions $dM/dlnD_p$ of all analyzed chemical constituents: inorganic ions, levoglucosan and total carbon. The different icons indicate a specific set of impactor filters and the different colors characterize a specific season of the year (winter - blue, spring - green, summer - red, autumn - gray; exception: yellow - summer, sample type 'sea'; also consider table 1).

Figure 3 highlights the relative contribution of the main constituents (NH_4^+, NO_3^-, SO_4^{2-}, TC, Na^+, Cl^-) for four typical impactor samples. Figure 3 (a) and (b) compare in more detail the mass fractions of a sample collected in spring (SP16_L1) to a sample collected in autumn (AU15_L2) to highlight seasonal differences. Figure 3 (c) and (d) show two filter sets collected

https://doi.org/10.5194/egusphere-2026-2593
Preprint. Discussion started: 23 June 2026

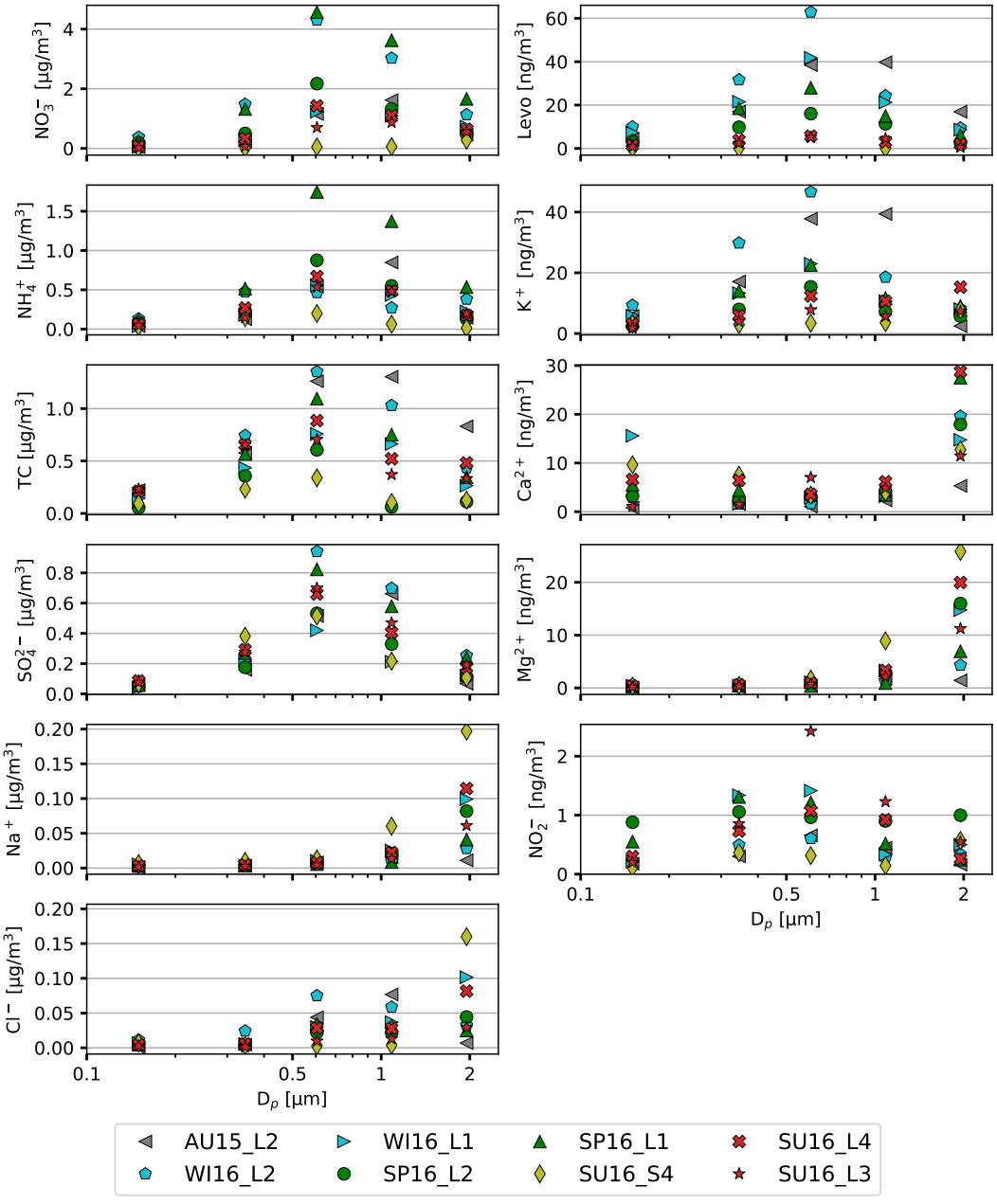

Figure 2. Mass size distributions of TC and inorganic ions ($dM/dlnD_p$): The shown impactor filter samples are from different seasons of the year. The color coding is as follows: winter - blue, spring - green, summer - red, autumn - gray; exception: yellow - summer, sample type 'sea'; cf. figure B1 for concentrations in mol/m^3; also consider table 1

https://doi.org/10.5194/egusphere-2026-2593
Preprint. Discussion started: 23 June 2026

in summer during the same time period; one set from the land (SU16_L4) and the other from the sea wind sector (SU16_S4). In addition the 72-hour back-trajectories (HYSPLIT trajectory model, time resolution one hour) are shown for each filter set.

As observed in earlier studies (Weijers et al., 2011; Mensah et al., 2012; Schlag et al., 2016) in the Netherlands the largest contribution to the aerosol particle mass comes from nitrate, ammonium and total carbon. The outflow aerosol from the land to the sea is dominated by ammonium nitrate as the main water soluble species. A main reason for the large influence of ammonium nitrate is the combination of intensive agriculture, responsible for high ammonia emissions, and the high traffic and industrialization, which emit nitrogen oxides. Most inorganic components show the highest mass concentrations at a size range between 0.5 µm and 1 µm, indicative of aged aerosol. This shows that the measurement site is influenced mainly by long range transport and not so much by local sources. The size distribution changes with air mass origin (Turšič et al., 2006) and residence time in the atmosphere, as can be seen comparing the filter set from autumn with the set from summer. For the autumn sample, the back-trajectories (see figure 3) show a long residence time over continental Europe and the mode of the mass distribution is at large particle diameters of around 1 µm. The summer sample on the contrary mostly has a much shorter residence time over land close to the sampling site and the mode of the size distribution is at smaller diameters of around 0.6 µm.

Particulate ammonium is the main cation to neutralize the most important atmospheric anions to form ammonium nitrate, ammonium sulfate and ammonium chloride. Formation of ammonium nitrate requires high concentrations of NH_3, because the more stable ammonium sulfate is preferentially produced. Ammonium nitrate is semi-volatile and consequently the mass concentration of particulate nitrate depends on temperature, with lower concentration in summer compared to the colder periods of the year. Especially high particulate nitrate concentrations occur at the end of the winter period (WI16_L2) and in spring with maximum concentrations between 0.5 µm and 1 µm. The highest mass concentrations of ammonium can be found in spring for particle sizes ranging from 0.44 µm to 1.4 µm, related to fertilizer use. The lowest concentrations are observed for samples from the marine sector, with the lowest relative contribution to the mass of the particles from the highest size range. Otherwise seasonal differences in concentration are not very strong. Currently, it is up for debate if reducing emissions of NH_3 or NO_x are more beneficial for reducing particulate matter (Gu et al., 2021; Guo et al., 2018; Jonson et al., 2022). However, our data show especially high contributions of ammonium nitrate to particulate matter, when ammonia emissions through fertilizer use are high in spring. Since NO_x emissions are much more constant over the year, this indicates that high ammonia is at least partially a limiting factor for ammonium nitrate formation.

The particle mass concentration of sulfate does not show any distinct seasonal variation. In figure 2 the total mass of sulfate is shown. The proportion of non-sea salt sulfate was calculated with sodium as a reference for sea salt and was found to be more than 97 % for all particle sizes except the largest size range for the 'land' filter set. Aerosol particles from the largest size range (1.4 µm-2.5 µm) show a clear impact from sea salt emission sources with a proportion of up to 21 % sulfate from sea salt and mainly for filter sets (e.g. in figure 3 (c)) under the influence of regional and coastal air masses. The 'sea' filter set has a proportion of 7 % sulfate mass from sea salt in the size range of 0.77 µm to 1.4 µm and 46 % in the size range of 1.4 µm to 2.5 µm. For the remaining particle size ranges of the 'sea' filter set the non-sea salt sulfate mass represents more than 98 % of total sulfate. Furthermore for the 'sea' filter set, sulfate is the main component next to TC for all sizes besides the largest

https://doi.org/10.5194/egusphere-2026-2593
Preprint. Discussion started: 23 June 2026

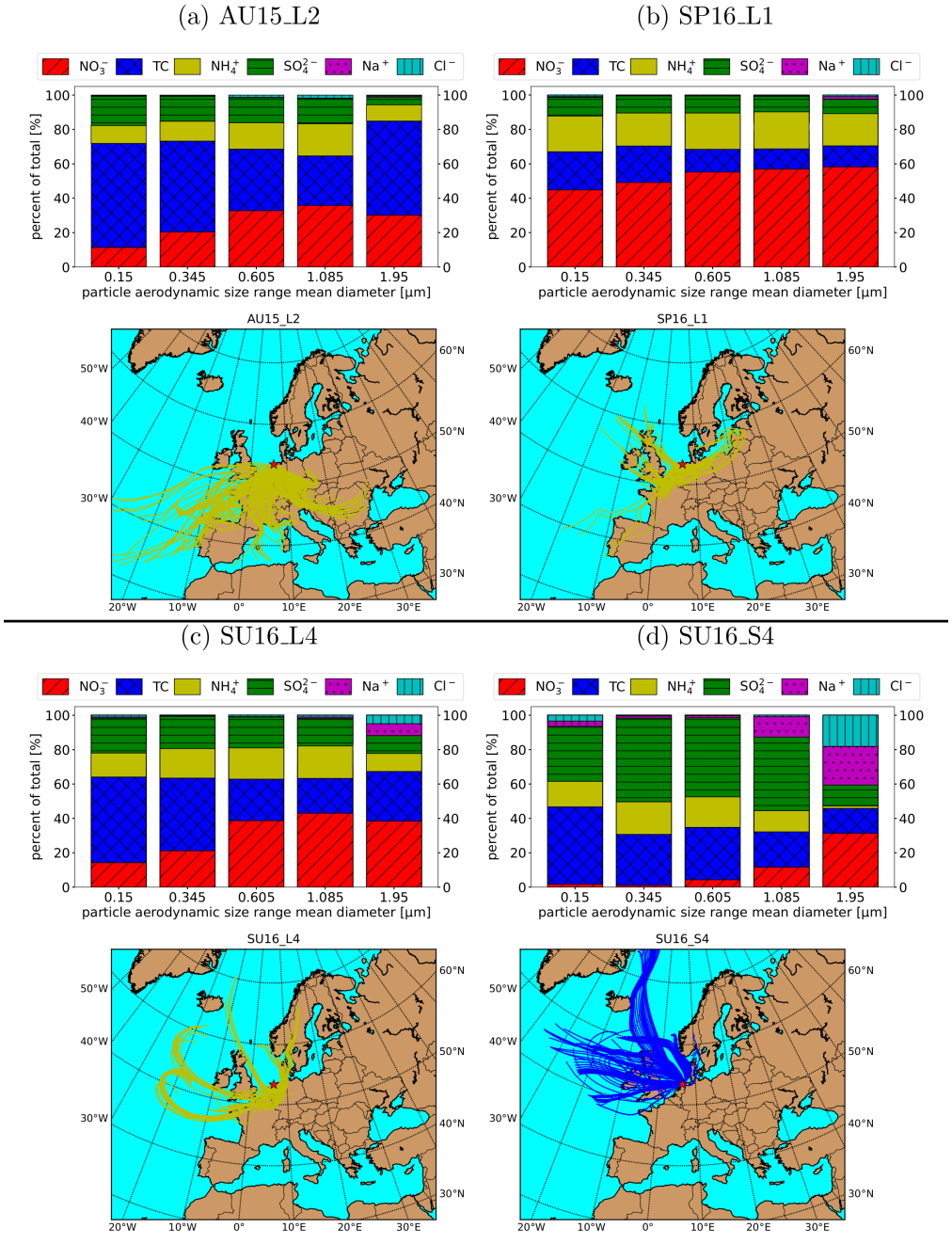

Figure 3. Aerosol mass contribution of the main constituents (NH_4^+, NO_3^-, SO_4^{2-}, TC, Na^+, Cl^-) in dependence of the particle size: The full bar (100 %) is the sum of the six constituents. Shown is a filter set from autumn (a) and one from spring (b). In the bottom a filter set with continental influence (c) is compared to a set with marine influence (d), both sets are collected in the same time period. For each filter set the 72-hour back-trajectories (HYSPLIT trajectory model, time resolution one hour) are shown.

https://doi.org/10.5194/egusphere-2026-2593
Preprint. Discussion started: 23 June 2026

collected size range. For sulfate aerosols, the ocean itself is a source with e.g. a total concentration of non-sea salt SO_4^{2-} of around 43 ng/m^3 on average for a remote station on the Svalbard Islands (Moroni et al., 2016). The 'sea' filter shows much higher SO_4^{2-} concentrations than this, therefore the combustion of fossil fuels by ship engines as an important emission source of the precursor gas SO_2 significantly contributes to sulfate concentrations. Since also TC mass concentrations are above the marine background concentrations, this supports ship emission as an important pollution source for this coastal location. In general, sulfate is the only major species (except for NaCl), where the absolute mass concentrations of the 'sea' filter is within the range of the 'land' filters and even exceeds the 'land' filters. Therefore most likely ship emissions are also a very relevant source not only locally, but for coastal locations in the Netherlands in general. The absolute concentrations of ammonium sulfate are much lower than TC and ammonium nitrate concentrations due to successful reduction of significant sources, like the industrial sector, by legal restrictions.

The total carbon mass shows higher concentrations in winter and autumn, which is most likely due to domestic biomass burning with the starting cold season. Potassium and levoglucosan, typical biomass burning tracers, also show clearly higher values in autumn and winter and lower values in summer and for the 'sea' filter set. Local and regional sources seem to make a significant contribution, because these tracers are especially enriched in the lower size ranges compared to the other analyzed components. The contribution of carbon from traffic emissions is assumed to be constant throughout the seasons. Local traffic emissions would cause elevated TC mass concentrations in the lower size ranges, as the combustion of fuel produces small aerosol particles. Our samples do not show this influence, which underlines the rural character of the measurement site. The 'sea' filter set, which was collected in summer, shows the lowest TC mass concentrations overall, but for the smallest size range TC concentrations are comparable to other samples. The main contributor here are likely ship emissions. In general, one would expect for a rural station higher TC concentrations in summer than in winter or autumn as biogenic secondary organic material contributes strongly to the aerosol mass. The measured concentrations do not show this and it was also not observed in earlier studies in the Netherlands (Dusek et al., 2017). The main reason here is probably the higher planetary boundary layer in summer than in the colder seasons. However, in the smallest two size classes, the mass concentrations of TC in the summer are comparable to or even higher than those in autumn and winter. This indicates, that biogenic SOA, produced regionally in the Netherlands during the summer, probably contributes more strongly to smaller particle sizes. This is supported by air mass back trajectories, which during the summer show air mass origin over the Atlantic and transport over the Benelux and Northern France resulting in regional pollution advected to the site. In autumn, the air is coming from central Europe representing integrated European outflow and much longer aging times. In general, in summer more stable weather conditions cause the transport of likely cleaner air masses from the main southwest wind direction. Whereas in autumn the atmosphere over Europe experiences the passage of more low pressure systems, so that the transport of air to the station is less predictable.

Sea salt is a source of the following analysed ions, stated from the highest to the lowest proportion by weight appearing in sea salt: chloride (Cl^-), sodium (Na^+), sulfate (SO_4^{2-}), magnesium (Mg^{2+}), calcium (Ca^{2+}), potassium (K^+) (Millero, 1996). Particles with diameters > 1 µm account for most of the PM2.5 sea salt aerosol mass, which is reflected in the aerosol mass size distributions shown in figure 2. Therefore, even though sea salt can significantly contribute to PM2.5, the contributions to the sub-micron range are very low. Obviously the 'sea' filter set shows the highest chloride, sodium and magnesium mass

https://doi.org/10.5194/egusphere-2026-2593
Preprint. Discussion started: 23 June 2026

concentrations for the highest size range, where the sodium chloride mass accounts for 40 % of the total constituents (figure 3 (d)). Even the 'land' filter set from the same time period (SU16_L4) shows a significant contribution from sea salt for the highest size range, which is related to air masses originating over the sea before crossing land as shown by the corresponding trajectories.

Despite the fact that chloride takes up the largest mass proportion of the sea salt constituents, its mass concentration or rather the concentration in mol/m^3 (see figure B1) is lower than sodium for the largest size range in the coastal aerosol samples. The difference is even clearer for the impactor stages with mean diameters of around 0.6 µm and 1 µm (see figure B1), where sodium shows elevated values in the 'sea' filter compared to the other samples, but chloride does not. This is evidence for the ageing of sea spray by reaction with nitric acid to form gas-phase hydrogen chloride (HCl) and particulate-phase sodium nitrate ($NaNO_3$) (Warneck, 1999), even in the relatively clean environment of the Wadden Sea coast. Since these samples are taken directly on the coast, this reaction must occur very rapidly after the air mass makes contact with the coast. For the largest size rage, the chloride is much less depleted than for the smaller sizes.

In the middle size ranges (mean diameters of around 0.35 µm and 1 µm), chloride mass concentrations (cf. concentrations in mol/m^3 in figure B1) are higher than sodium mass concentrations for the 'land' filters, especially in winter and autumn. Chloride is then likely present in the form of ammonium chloride (NH_4Cl), a semi-volatile compound, which explains higher concentrations in the colder seasons. Magnesium shows a very similar size distribution as sodium with the largest values for the 'sea' filter set and at larger particle sizes, indicating that its main source is sea spray.

Calcium has a very distinct mass size distribution with elevated values for the lowest and the highest size range. An emission source for calcium is sea salt, but this has only a minor contribution. Another important source is mineral crust material, especially limestone (Warneck, 1999), which produces primary coarse mode particles by wind erosion. In general dry conditions and high wind velocities cause more mineral crustal material to become airborne. This explains the high particle mass concentrations for the largest size range and increased values for winter and spring for this size range. Elevated values for the lowest size range could occur, because of particle bounce in the impactor, which causes large particle not to be collected on their size corresponding impaction plate, but to bounce off and eventually end up on the back-up filter (lowest size range). This happens especially with dry particles, such as mineral dust. However, particle bounce is less likely on quartz fibre filter compared to smooth substrates. The reason for elevated particle mass concentrations of calcium in the lowest size range remains unclear.

3.2 Isotopic analysis of organic carbon

Figure 4 shows the fraction modern of organic carbon ($F(^{14}C, OC)$) as a function of particle size for the analyzed aerosol filter samples. An $F(^{14}C)$ of 0 % corresponds to pure fossil origin of the OA, whereas $F(^{14}C)$ of around 100 % indicates biogenic origin. The particle size is shown as the geometric mean of the lower and the upper cut-off-size of the relevant impactor stage. If two stages were combined in order to have enough material for the analysis of the $^{14}C/^{12}C$ ratio (i.e. for some spring and summer samples), the geometric mean of the lower cut-off diameter for the smaller stage and the upper cut-off for the larger stage is used. Some of the autumn filter samples have been analyzed twice and the values show a high repeatability for $F(^{14}C, OC)$.

https://doi.org/10.5194/egusphere-2026-2593
Preprint. Discussion started: 23 June 2026

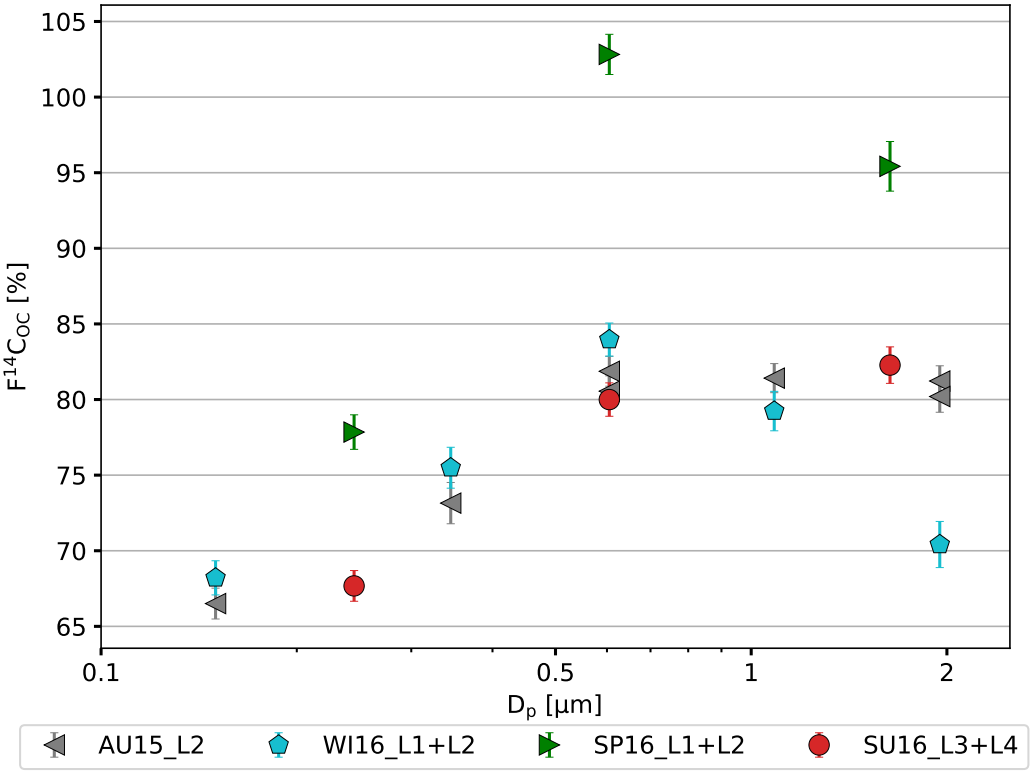

Figure 4. Fraction modern of organic carbon ($F(^{14}C, OC)$) in dependence of the particle size range: The particle size is shown as the geometric mean of the lower and the upper cut-off-size of the relevant impactor stage. In case filter from different impactor stages were combined the geometric mean of the lower cut-off diameter for the smaller stage and the upper cut-off for the larger stage is used. The shown impactor filter samples are collected in different seasons of the year. The color coding is as follows: winter - blue, spring - green, summer - red, autumn - gray; also consider table 1

The organic carbon of all filter samples is clearly dominated by modern sources, as the lowest $F(^{14}C, OC)$ value is about 67 %. The highest $F(^{14}C, OC)$ occurs in spring with a value of about 103 % in the size range that covers particle sizes from 0.44 µm to 0.77 µm, which is very close to the $F(^{14}C)$ of atmospheric carbon dioxide of approximately 104 % (Levin et al., 2010). In general, the impactor samples taken in spring show elevated $F(^{14}C, OC)$ compared to the other seasons. For all seasons $F(^{14}C, OC)$ is lowest at small particle sizes and increases towards the particle size range of 0.44 µm to 0.77 µm. Usually, a slight decrease for the larger particles can be observed. Even for this relatively remote coastal site in the Netherlands quite far from major roads and urban centres a clear influence of fossil sources on the smaller particles is evident. These particles most likely originate from regional vehicular and/or ship traffic. For the winter samples this trend is clearest. $F(^{14}C, OC)$ is 68 % for the smallest size range, increases to 84 % for the middle size range and decreases to 70 % for the largest size range. This is the first time this significant size dependence in fossil contribution to OC has been demonstrated in Western

https://doi.org/10.5194/egusphere-2026-2593
Preprint. Discussion started: 23 June 2026

Europe. In contrast a study in a megacity in China showed no significant size dependence in fossil contribution to OC (Ni et al., 2022).

The main sources for contemporary carbon are biogenic SOA and biomass burning, but previous studies (Dusek et al., 2017; Yttri et al., 2011; Genberg et al., 2011) show, that also primary biogenic particles, e.g. pollen fragments, or cooking emissions (Zotter et al., 2014) can contribute to high values of the fraction modern. In this remote area cooking is not a very likely source as there are only small villages within 20 km of the site.

Higher values of $F(^{14}\text{C, OC})$ in spring compared to all other seasons were also observed in another seasonal study of radiocarbon in the Netherlands (Dusek et al., 2017). In this study, $F(^{14}\text{C, OC})$ was analyzed for PM2.5 without any size dependence. Average values of $F(^{14}\text{C, OC})$ for summer (71 %), autumn (78 %) and winter (74 %) varied within a narrow range of about ± 4 %, but the average $F(^{14}\text{C, OC})$ in spring was much higher with a value of 89 %. This is roughly comparable to the weighted average over the whole size range in our study (summer 75 %, autumn 78 %, winter 76 %, spring 90 %). Dusek et al. (2017) discuss, that elevated values of $F(^{14}\text{C, OC})$ in spring are most likely caused by biogenic SOA and prevalent during the growing season. In the highly agricultural region of the Netherlands maximum biogenic SOA production thus seems to occur in spring and not in summer, such as in other, more forested, regions.

$F(^{14}\text{C})$ of SOA depends on the origin of the precursor gases, that are involved in forming secondary organic carbon. If these gases primarily originate from fossil sources, then the formed particulate matter will have low $F(^{14}\text{C})$ values. In our case an influence from modern sources on SOA is more prominent, as $F(^{14}\text{C, OC})$ is above 65 % for all size ranges and sources surrounding the sampling station are predominantly biogenic. Even though biogenic sources and SOA production are mainly enhanced in warmer seasons, $F(^{14}\text{C, OC})$ in winter samples shows similar values to summer samples. This is likely caused by biomass burning as an important source for OC in winter and autumn, which increases $F(^{14}\text{C, OC})$. Biomass burning in the Netherlands mostly occurs in residential heating with fire wood or pellets. This type of heating is more common in rural areas than in cities.

Figure 5 shows the $\delta(^{13}\text{C})$ values of organic carbon ($\delta(^{13}\text{C, OC})$) as a function of particle size for different desorption temperatures (200 °C, 350 °C, 650 °C). The color coding for the different seasons of the year is the same as used in figure 2 (winter - blue, spring - green, summer - red, autumn - gray; exception: yellow - summer, sample type 'sea'; see table 1). The shaded horizontal areas show the range of typical $\delta(^{13}\text{C, OC})$ values for particles emitted from primary sources, as expected for this region (Zenker et al., 2020; Masalaite et al., 2026). Non fossil sources, namely biomass burning, are shown in green and traffic emissions are shown in gray. For biomass burning aerosol the range encompasses emissions from burning of alder, oak, birch, ash and Quercus ilex (oak) wood. Theses biomass burning sources represent characteristic material for heating, that can be bought, e.g. in the form of pellets, on the Dutch market. Traffic emissions were measured on filters collected in a tunnel of a main city traffic street in Naples and directly collected from a city bus exhaust. These samples are selected as they represent a typical mixture of traffic emissions, that can be expected in Western Europe. Unfortunately not so many source reference measurements are published so far for this type of analysis with the different temperature steps, especially focused on the Western European region.

https://doi.org/10.5194/egusphere-2026-2593
Preprint. Discussion started: 23 June 2026

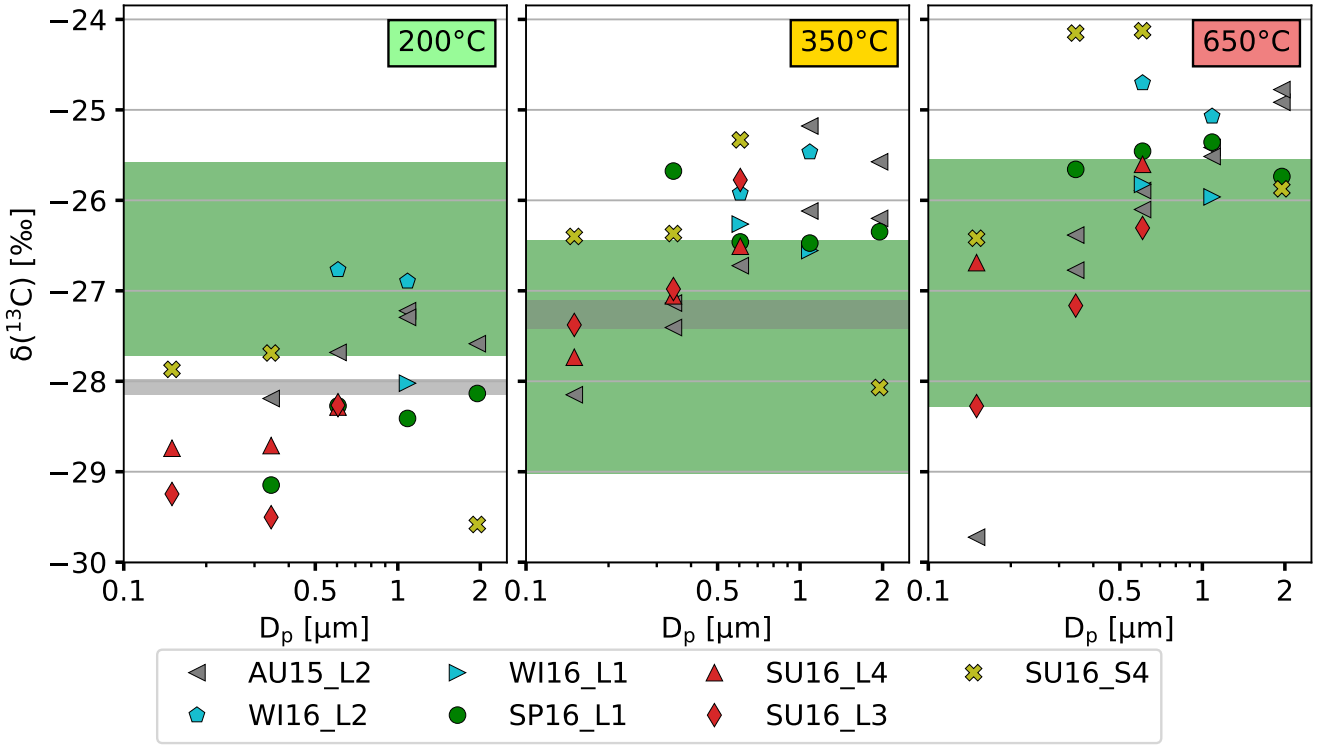

Figure 5. $\delta(^{13}C, OC)$ depending on particle size and temperature step (200 °C, 350 °C, 650 °C): The shown impactor filter samples are from different seasons of the year. The color coding is as follows: winter - blue, spring - green, summer - red, autumn - gray; exception: yellow - summer, sample type 'sea'; also consider table 1. The typical uncertainty of the values is 0.22 ‰, as explained in section 2.4.

For some impactor filter sets $\delta(^{13}C, OC)$ values were not available for every particle size, as e.g. the measurement did not satisfy the quality control or not enough filter material was left after chemical analysis and the analysis of the $^{14}C/^{12}C$ ratio. On that account for some seasons, especially winter, it is not possible to draw a comprehensive conclusion for the trends of the $\delta(^{13}C, OC)$ values over the whole particle size range. The measurement of the autumn filter set (AU15_L2) was repeated for some size ranges. Most of these $\delta(^{13}C, OC)$ values are repeatable within the measurement uncertainty.

An overall increase of $\delta(^{13}C, OC)$ can be observed with increasing desorption temperature. This was also observed in previous studies on ambient aerosol (Ni et al., 2023, 2022; Masalaite et al., 2020). Since the same increase is typically not necessarily observed in source samples (Zenker et al., 2020; Yao et al., 2022; Vernooij et al., 2022), we conclude that it is related either to differences in contributing sources at the investigated desorption temperatures or to different atmospheric transformation processes that influence the particular OC fractions.

Considering the particle size distribution, the $\delta(^{13}C, OC)$ values tend to increase with increasing particle size. This increase in $\delta(^{13}C, OC)$ with increasing particle size is more pronounced for higher desorption temperatures and less evident at 200 °C. At higher temperatures many $\delta(^{13}C, OC)$ values, especially for the size range 0.44 µm to 0.77 µm and larger, are higher than the

https://doi.org/10.5194/egusphere-2026-2593
Preprint. Discussion started: 23 June 2026

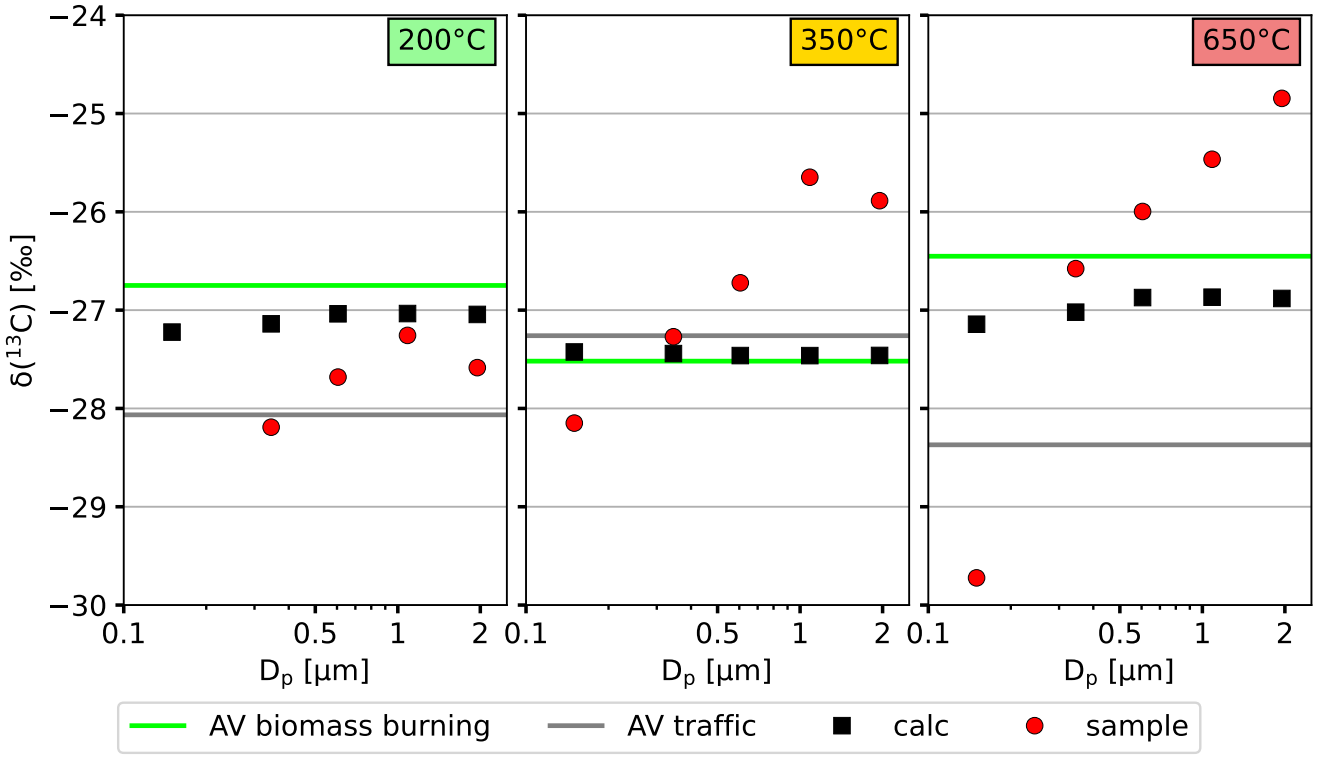

Figure 6. Comparison of averaged analyzed $\delta(^{13}C, OC)$ of samples from autumn (AU15_L2) (red) and thereoretical calculated $\delta(^{13}C, OC, prim)$ (black): The calculation is based on the $F(^{14}C, OC)$ of the respective filter set and average values of $\delta(^{13}C, OC)$ from source filter (biomass burning and traffic). Average $\delta(^{13}C, OC)$ of the source filter are shown as lines for the different temperature steps (biomass burning - green line; traffic - gray line).

$\delta(^{13}C, OC)$ values of the possible primary sources. The filter sets from summer and autumn show a clearer increase of $\delta(^{13}C,$ OC) with increasing particle size, especially for 350 °C and 650 °C. Ni et al. (2022) found an increasing mass fraction of OC at 650 °C for larger particles and also higher $\delta(^{13}C, OC)$(650 °C) values with increasing particle size. The observation was explained with photochemical aging of the aerosol and as it especially occurred in combination with low and moderate $PM_{2.5}$ pollution events, where regional aged aerosol contributes significantly to urban pollution. At 200 °C most $\delta(^{13}C, OC)$ values are lower compared to the primary sources (horizontal green and gray areas). This is especially the case for filters from spring and summer, where $\delta(^{13}C, OC)$ values are all lower than the values of the primary sources. Lower values of $\delta(^{13}C, OC)$ for the OC fraction desorbed at 200 °C were also found for samples from the Tibetian Plateau (Ni et al., 2023), different sampling areas in Lithuania (Masalaite et al., 2020) and samples collected in Beijing (Ni et al., 2022).

Figure 6 compares calculated $\delta(^{13}C, OC, prim)$ (black squares) based on a hypothetical mixture of only primary sources (in this case, traffic emissions and biomass burning) to the measured $\delta(^{13}C, OC)$ (red circles) for autumn. The primary source mix is estimated based on the $F(^{14}C, OC)$ values from figure 4, which give the relative contribution of fossil and modern

https://doi.org/10.5194/egusphere-2026-2593
Preprint. Discussion started: 23 June 2026

sources to OC. For example a $F(^{14}\mathrm{C}, \mathrm{OC})$ value of 80 % means, that roughly 80 % of OC originated from modern sources and 20 % originated from fossil sources. The $\delta(^{13}\mathrm{C}, \mathrm{OC})$ values assigned to fossil and modern primary sources are the values for vehicular sources and biomass burning shown in figure 5 as the shaded areas. For the calculation the respective $\delta(^{13}\mathrm{C}, \mathrm{OC})$ values of the sources are averaged and are depicted as horizontal lines in figure 6 for every temperature step. Modern sources, here biomass burning sources, are shown as green line and fossil sources, in this case traffic sources, are shown as gray line. The calculation of the theoretical $\delta(^{13}\mathrm{C}, \mathrm{OC}, \mathrm{prim})$ is summarized in the following equation:

$$\delta(^{13}\mathrm{C}, \mathrm{OC}, \mathrm{prim}) = \frac{\mathrm{F}(^{14}\mathrm{C}, \mathrm{OC}, \mathrm{sample})}{104\%} \cdot \delta(^{13}\mathrm{C}, \mathrm{OC}, \mathrm{modern}) + \left(1 - \frac{\mathrm{F}(^{14}\mathrm{C}, \mathrm{OC}, \mathrm{sample})}{104\%}\right) \cdot \delta(^{13}\mathrm{C}, \mathrm{OC}, \mathrm{fossil}) \quad (3)$$

104 % is the $F(^{14}\mathrm{C})$ value of atmospheric carbon dioxide (Levin et al., 2010).

The most obvious observation from figure 6 is the low variability (< 1 ‰) of the calculated $\delta(^{13}\mathrm{C}, \mathrm{OC}, \mathrm{prim})$ with changing particle size compared to values of the real sample. The calculated $\delta(^{13}\mathrm{C}, \mathrm{OC}, \mathrm{prim})$ do not vary strongly with the temperature step or particle size. This is also in line with findings of a study investigating the $\delta(^{13}\mathrm{C})$ of OC in primary emissions (Zenker et al., 2020), where $\delta(^{13}\mathrm{C}, \mathrm{OC})$ did not vary much with changing desorption temperature. Basically, if the organic aerosol were dominated by a primary source mix, without the contribution of SOA or aging processes, we would expect $\delta(^{13}\mathrm{C}, \mathrm{OC})$ to vary only in a relatively narrow range.

On the contrary, the $\delta(^{13}\mathrm{C}, \mathrm{OC})$ of the sampled aerosol particles show an increase with increasing particle size. This means smaller, on average less aged particles have lower $\delta(^{13}\mathrm{C})$ values than larger particles. With respect to desorption temperature, at 200 °C all values of $\delta(^{13}\mathrm{C}, \mathrm{OC})$ of the samples are depleted compared to the calculated values. For the higher temperatures (350 °C and 650 °C) the measured $\delta(^{13}\mathrm{C}, \mathrm{OC})$ values are, except for the smallest particle size range, enriched compared to the theoretical $\delta(^{13}\mathrm{C}, \mathrm{OC}, \mathrm{prim})$.

The depletion at 200 °C is most likely caused by the influence of recently formed SOA as it tends to desorb at lower temperatures (Meusinger et al., 2017). Due to the kinetic isotope effect, $^{12}\mathrm{C}$ is preferred during the formation of SOA from the precursor gas and accumulates in the reaction products that condense on the aerosol. As a consequence the $^{13}\mathrm{C}/^{12}\mathrm{C}$ ratio in the formed SOA will be less than in the precursor gas and likely less than in the primary organic particle matter. If incomplete, this process leads to a depletion of $^{13}\mathrm{C}$ (i. e. low $\delta(^{13}\mathrm{C})$ values) in the particle phase of the aerosol. The original primary particle, not influenced by atmospheric transformation processes, is in our case represented by the theoretical $\delta(^{13}\mathrm{C}, \mathrm{OC}, \mathrm{prim})$. SOA condenses on all particles, irrespective of their size. However, proportionally more SOA is added to the smaller particles. The lower $\delta(^{13}\mathrm{C}, \mathrm{OC})$ values of the smaller particles observed in this study are consistent with this fact. Since SOA can also contain low- and non-volatile compounds, a similar effect and size dependence can also be seen for higher desorption temperatures. However, for higher desorption temperatures only the smallest particles are depleted in $^{13}\mathrm{C}$ compared to the estimated primary signature. As shown in figure 5, $\delta(^{13}\mathrm{C}, \mathrm{OC})$ is especially depleted in spring and summer, compared to the other seasons and the primary source values. This is consistent with enhanced SOA formation in these warmer seasons.

The enrichment of the measured $\delta(^{13}\mathrm{C}, \mathrm{OC})$ compared to $\delta(^{13}\mathrm{C}, \mathrm{OC}, \mathrm{prim})$, especially at 650 °C, is most likely caused by aerosol aging. Photochemical aging causes a net loss of organic carbon from the particle and the isotopically lighter carbon $^{12}\mathrm{C}$ is preferentially lost. If the particle is only partially oxidized, the remaining carbon in the particle is enriched in $^{13}\mathrm{C}$

https://doi.org/10.5194/egusphere-2026-2593
Preprint. Discussion started: 23 June 2026

compared to carbon of the original particle. As reflected by the $\delta(^{13}C, OC)$ of the samples (see also figure 5), aerosol aging is more relevant for larger particles (accumulation mode) as these particles have a longer residence time in the atmosphere and therefore are involved in long range transport. The smaller particles (see figure 5) show $\delta(^{13}C, OC)$ close to the primary emission sources at higher desorption temperatures. The increase of the measured $\delta(^{13}C, OC)$ values with particle size is much stronger at 650 °C than for lower temperatures. Especially for this filter set from autumn the influence of aged regional aerosol is larger than the effect of SOA production.

4 Conclusions

Size-resolved aerosol filter samples in the sub-micrometer size range were collected in a one year long sampling campaign at a site close to the Wadden Sea in the Netherlands. The filter samples were analyzed for mass concentration of different inorganic ions and total carbon, as well as for the ^{13}C signature of organic carbon desorbed at three different temperature steps (200 °C, 350 °C, 650 °C) and the ^{14}C isotopic signatures of total OC to investigate seasonal changes of the chemical composition of aerosol particles and related atmospheric transformation processes.

The objective of this study was to characterize the seasonal, air mass and size dependent variation of the aerosol chemical composition at a site close to the Wadden Sea in the Netherlands. Chemical analysis of size-resolved aerosol filter samples in the sub-micrometer size range shows that the largest contributions to aerosol particle mass are from nitrate, ammonium and carbon. This is in line with earlier studies and is typical for the Netherlands where the agricultural sector is a major source for pollutants, especially at rural sites.

Most ion mass concentrations show a typical seasonal trend depending on sources and the volatility of the formed inorganic salts. For example, particulate nitrate shows lower mass concentrations in summer compared to winter, because temperatures are higher in summer and ammonium nitrate, the main form of nitrate in this region, is semi-volatile.

In contrast, sulfate does not display any seasonal changes, because sulfuric acid and ammonium sulfate have a very low volatility. A similar mass size distribution of sulfate was observed during wind directions from both land and sea. As ship emissions are the main source of non-sea salt sulfate over sea, this emphasizes the importance of ship emissions as a source of sulfate in the Netherlands. Outside of harbor regions, it has to our knowledge not been observed that aerosols in marine air masses have comparable sulfate concentrations as in regional, continental air masses.

Inorganic ions, whose main emission source is sea salt, like chloride, sodium or magnesium, show a very distinct mass size distribution with elevated values for the largest size range. Even though NaCl is present in the PM2.5 mass, only a small mass fraction occurs in the sub-micron range.

Compared to the inorganic ions, the size distribution of TC is shifted towards smaller sizes, such that particles with diameters < 250 nm can have up to two times higher TC mass fractions compared to the bulk aerosol. Since cloud condensation nuclei (CCN) are typically in this size range, the bulk aerosol composition is not representative for estimating CCN in this region.

A second objective of this study was to demonstrate the potential of carbon isotopes to provide more detailed insights into sources and processing of carbonaceous aerosols. The size distribution of $F(^{14}C, OC)$ shows a similar trend for all seasons

https://doi.org/10.5194/egusphere-2026-2593
Preprint. Discussion started: 23 June 2026

of the year with in general high values of larger than 67 %, which indicates that non-fossil sources are dominant. $F(^{14}C, OC)$ values in spring show even higher values, with the highest value of more than 100 % in the size range of 0.44 µm to 0.77 µm. This is the first time this significant size dependence in fossil contribution to OC has been demonstrated in Western Europe. In contrast a study in a megacity in China showed no significant size dependence in fossil contribution to OC. High values of $F(^{14}C, OC)$ in autumn and winter are likely caused by biomass burning for residential heating, especially as during these seasons the size distribution of levoglucosan is very similar to the size distribution of TC. The input from regional traffic is clearly visible in the size distribution of $F(^{14}C, OC)$ with lower values for the smallest size ranges, which correspond to the size range of primary traffic particles. The clearly modern values of $F(^{14}C, OC)$ for the different seasons, although similar, occur because of a combination of different effects; biomass burning in autumn and winter and SOA production from biogenic precursor gases in spring and summer. An earlier study in the Netherlands, that analyzed $F(^{14}C, OC)$ of PM2.5 without any size dependence showed a similar seasonal trend with higher values of $F(^{14}C, OC)$ in spring compared to all other seasons. It seems that in this highly agricultural region of the Netherlands the maximum biogenic SOA production occurs in spring and not in summer, such as in other, more forested, regions.

$\delta(^{13}C, OC)$ values increase with increasing desorption temperature (200 °C, 350 °C, 650 °C) and larger aerosol particles tend to show higher $\delta(^{13}C, OC)$. This is consistent with the theory that SOA formation can be traced by low $\delta(^{13}C)$ values, whereas photochemical aging by increasing $\delta(^{13}C)$ values. Similar observations were also made in earlier studies for other regions of the world. This holds promise that ^{13}C signatures can be used to gain more quantitative insights into atmospheric formation and processing of organic aerosol.

The broader implications of the chemical composition and OC sources pertain especially to the European outflow over the North Sea, where it will impact the radiative balance and clouds. The outflow is characterized by high ammonium nitrate concentrations, which will have a major influence on cloud activation and radiative forcing, but it is currently not represented in climate models. On the other hand, the significant increase in the organic fraction at lower diameters shows that CCN concentrations will likely be overestimated, when they are only based on bulk chemical composition. We also show that the contribution of fossil sources to organic aerosol is minor. OC likely contains increasing contributions of SOA at smaller particle sizes especially in spring and summer, whereas the larger particles are highly aged. However, these conclusions are somewhat speculative at the moment. To get better insights into SOA contribution and the effect of aging require better source characterization and controlled laboratory studies into isotope effects of chemical processes.

Overall, the dataset highlights the strong size dependence of aerosol composition and carbon isotopes at coastal sites and demonstrates the potential of combined size-resolved chemical and isotopic measurements to better characterize sources and atmospheric transformation processes of organic aerosol.

Data availability. The dataset accompanying this publication is available at https://doi.org/10.5281/zenodo.19990975 (Zenker et al., 2026)

https://doi.org/10.5194/egusphere-2026-2593
Preprint. Discussion started: 23 June 2026

Appendix A

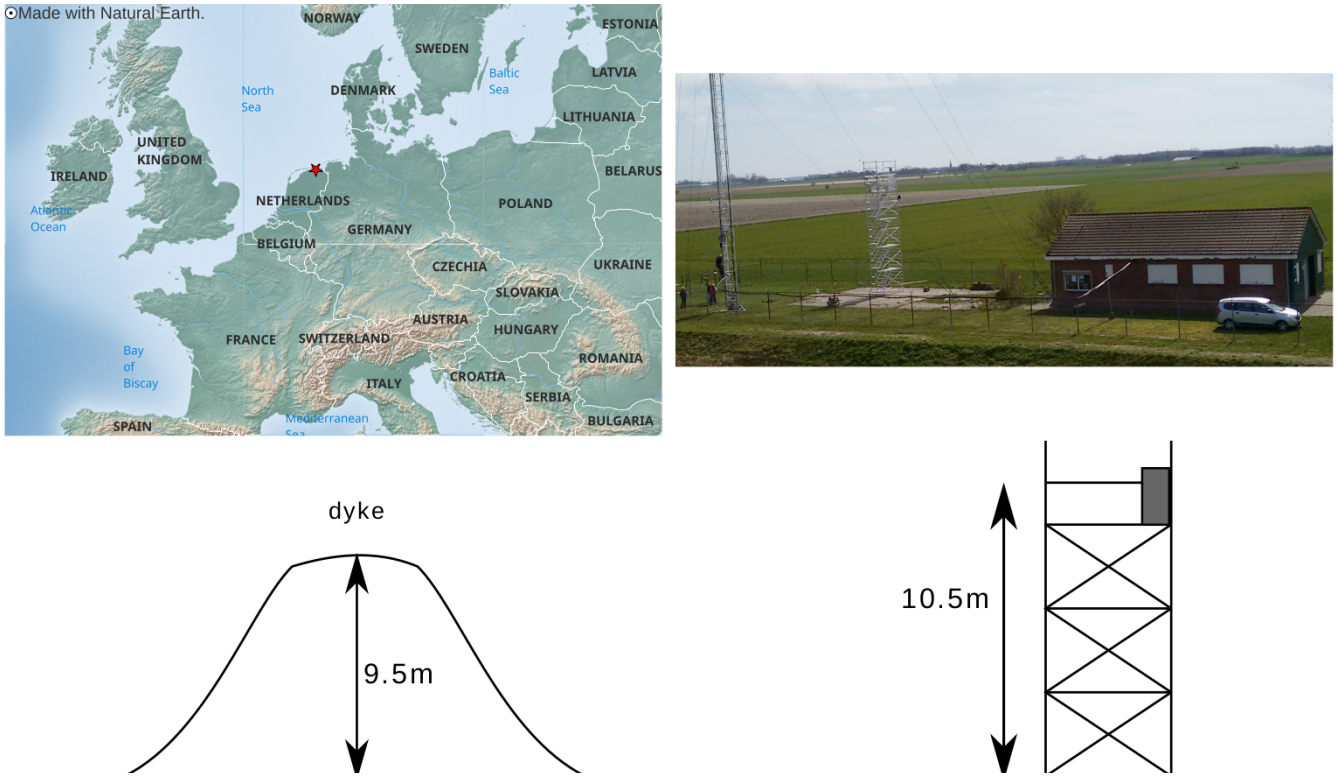

Figure A1. Sampling Site: top left shows the position within Europe, top right shows the measurement station Lutjewad and the bottom shows the proportion of the scaffolding, with the sampling equipment on top, to the dyke

https://doi.org/10.5194/egusphere-2026-2593
Preprint. Discussion started: 23 June 2026

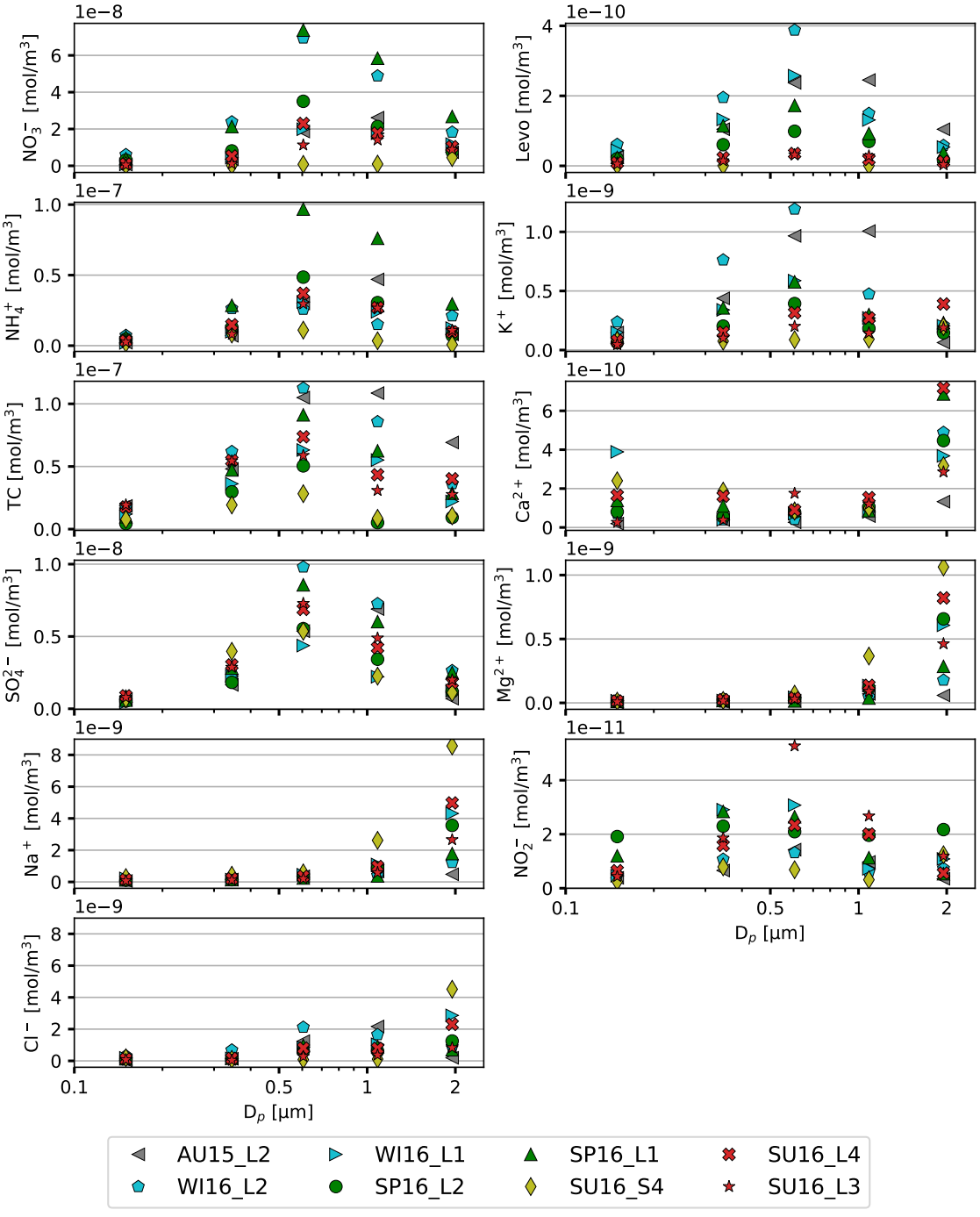

Figure B1. Size distributions of the amount of substance of TC and inorganic ions: The shown impactor filter samples are from different seasons of the year. The color coding is as follows: winter - blue, spring - green, summer - red, autumn - gray; exception: yellow - summer, sample type 'sea'; also consider table 1

https://doi.org/10.5194/egusphere-2026-2593
Preprint. Discussion started: 23 June 2026

(a) WI16_L1 (b) WI16_L2

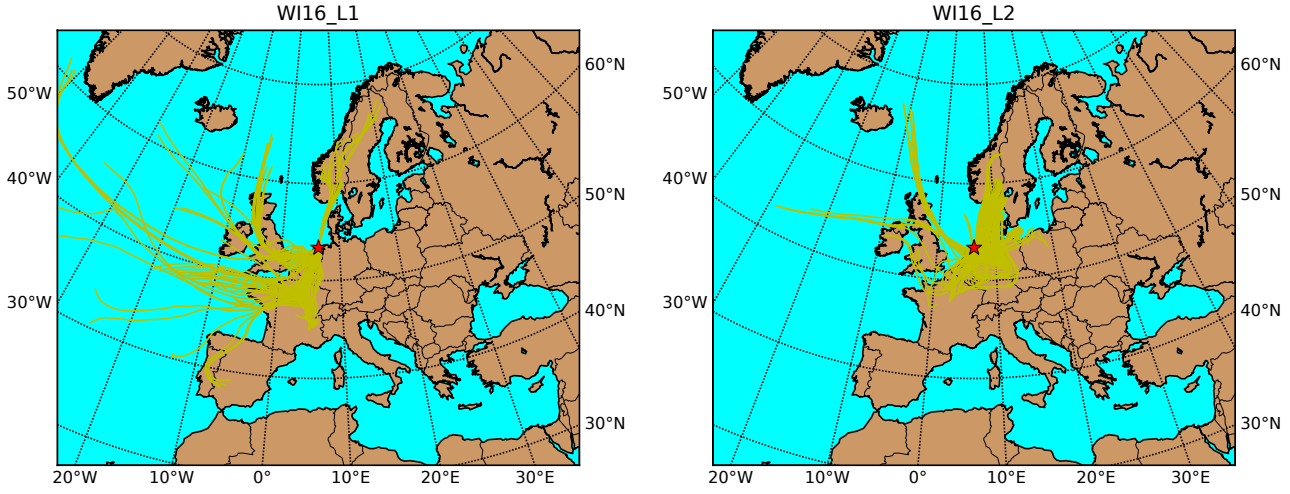

(c) SP16_L2 (d) SU16_L3

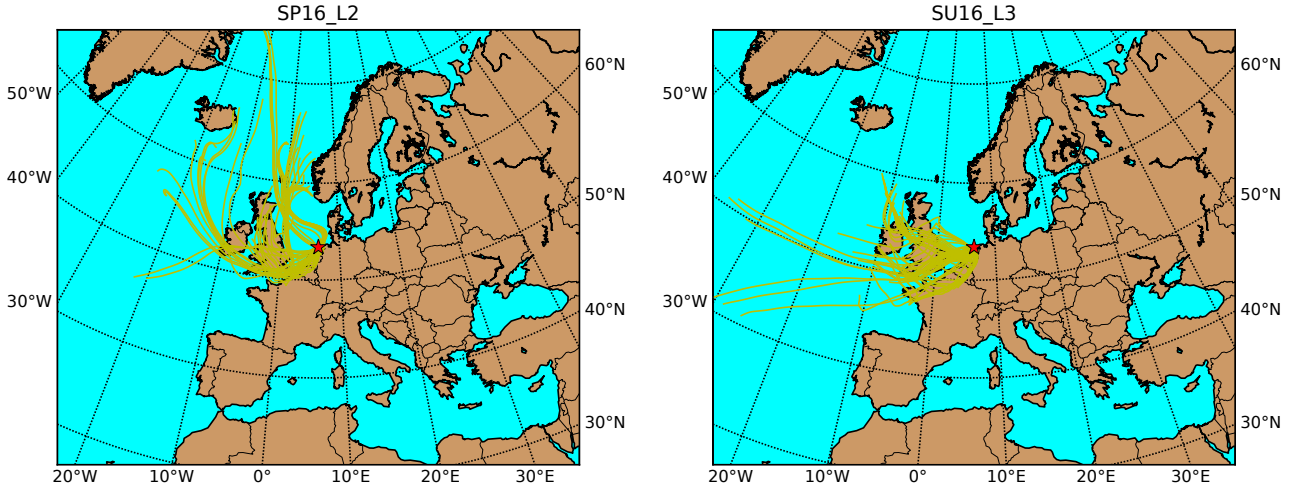

Figure C1. Supplement for figure 3: The 72-hour back-trajectories (HYSPLIT trajectory model, time resolution one hour) for the remaining filter sets from table 1.

https://doi.org/10.5194/egusphere-2026-2593
Preprint. Discussion started: 23 June 2026

Author contributions. Peter Redl and Anne Kasper-Giebl performed the experimental and data analysis for the chromatographic analysis at the Institute of Chemical Technologies and Analytics, Vienna University of Technology and provided valuable comments for the manuscript. Furthermore Anne Kasper-Giebl wrote the method description "Analyses of ions and levoglucosan". Ulrike Dusek conceived the idea and supervised the project and revised the manuscript. Katrin Zenker conducted the sampling campaign and performed the experimental and data analysis for the measurement of total carbon, $F(^{14}\text{C, OC})$ and $\delta(^{13}\text{C, OC})$ and wrote the main part of the manuscript.

Competing interests. We have no conflicts of interest to declare.

Acknowledgements. The authors like to thank Bert Kers, Marcel de Vries and Romke Tjoelker for their help during the measurement campaign. We thereby like to emphasize the importance of support from technical staff during scientific work. Furthermore we like to thank Henk Jansen for his daily technical support during laboratory measurements and Dipayan Paul and Marc Bleeker for conducting the AMS measurements. The authors also like to thank Anni E. Kortesmaa for her improvements of the ^{13}C measurement setup by including a reduction oven, Koen Oosterveen for further ^{13}C laboratory measurements and Max Cosjin for ^{14}C data corrections. This long-term measurement campaign could not have been accomplished without the research facility Lutjewad, part of the Ruisdael Observatory, which is co-financed by the Dutch Research Council (NWO; grant number 184.034.015). Such measurement stations are crucial for long and continuous atmospheric observations that allow to learn about atmospheric processes and to provide long data sets, which are essential for the development of atmospheric models.

https://doi.org/10.5194/egusphere-2026-2593
Preprint. Discussion started: 23 June 2026

References

Aerts-Bijma, A. T., Paul, D., Dee, M. W., Palstra, S. W. L., and Meijer, H. A. J.: AN INDEPENDENT ASSESSMENT OF UNCERTAINTY FOR RADIOCARBON ANALYSIS WITH THE NEW GENERATION HIGH-YIELD ACCELERATOR MASS SPECTROMETERS, Radiocarbon, 63, 1–22, https://doi.org/10.1017/RDC.2020.101, 2021.

Boucher, O., Randall, D., Artaxo, P., Bretherton, C., Feingold, G., Forster, P., Kerminen, V.-M., Kondo, Y., Liao, H., Lohmann, U., Rasch, P., Satheesh, S. K., Sherwood, S., Stevens, B., and Zhang, X. Y.: Clouds and Aerosols, in: Climate Change 2013: The Physical Science Basis. Contribution of Working Group I to the Fifth Assessment Report of the Intergovernmental Panel on Climate Change, edited by Stocker, T., Qin, D., Plattner, G.-K., Tignor, M., Allen, S., Boschung, J., Nauels, A., Xia, Y., Bex, V., and Midgley, P., chap. 7, p. 571–658, Cambridge University Press, Cambridge, United Kingdom and New York, NY, USA, ISBN ISBN 978-1-107-66182-0, https://doi.org/10.1017/CBO9781107415324.016, 2013.

Ceburnis, D., Garbaras, A., Szidat, S., Rinaldi, M., Fahrni, S., Perron, N., Wacker, L., Leinert, S., Remeikis, V., Facchini, M. C., Prevot, A. S. H., Jennings, S. G., Ramonet, M., and O'Dowd, C. D.: Quantification of the carbonaceous matter origin in submicron marine aerosol by ^{13}C and ^{14}C isotope analysis, Atmospheric Chemistry and Physics, 11, 8593 – 8606, https://doi.org/10.5194/acp-11-8593-2011, 2011.

Chesselet, R., Fontugne, M., Buat-Ménard, P., Ezat, U., and Lambert, C. E.: The origin of particulate organic carbon in the marine atmosphere as indicated by its stable carbon isotopic composition, Geophysical Research Letters, 8, 345–348, https://doi.org/10.1029/GL008i004p00345, 1981.

Donahue, N. M., Robinson, A. L., and Pandis, S. N.: Atmospheric organic particulate matter: From smoke to secondary organic aerosol, Atmospheric Environment, 43, 94 – 106, https://doi.org/https://doi.org/10.1016/j.atmosenv.2008.09.055, 2009.

Dusek, U., Hitzenberger, R., Kasper-Giebl, A., Kistler, M., Meijer, H. A. J., Szidat, S., Wacker, L., Holzinger, R., and Röckmann, T.: Sources and formation mechanisms of carbonaceous aerosol at a regional background site in the Netherlands: insights from a year-long radiocarbon study, Atmospheric Chemistry and Physics, 17, 3233–3251, https://doi.org/10.5194/acp-17-3233-2017, 2017.

Dusek, U., Cosijn, M. M., Ni, H., Huang, R.-J., Meijer, H. A. J., and van Heuven, S.: Technical Note: An Automated System for Separate Combustion of Elemental and Organic Carbon for 14C Analysis of Carbonaceous Aerosol, Aerosol and Air Quality Research, 19, 2604–2611, https://doi.org/10.4209/aaqr.2019.06.0287, 2019.

Fitzgerald, J. W.: Marine aerosols: A review, Atmospheric Environment. Part A. General Topics, 25, 533–545, https://doi.org/https://doi.org/10.1016/0960-1686(91)90050-H, 1991.

Fuzzi, S., Baltensperger, U., Carslaw, K., Decesari, S., Denier van der Gon, H., Facchini, M. C., Fowler, D., Koren, I., Langford, B., Lohmann, U., Nemitz, E., Pandis, S., Riipinen, I., Rudich, Y., Schaap, M., Slowik, J. G., Spracklen, D. V., Vignati, E., Wild, M., Williams, M., and Gilardoni, S.: Particulate matter, air quality and climate: lessons learned and future needs, Atmospheric Chemistry and Physics, 15, 8217–8299, https://doi.org/10.5194/acp-15-8217-2015, 2015.

Genberg, J., Hyder, M., Stenström, K., Bergström, R., Simpson, D., Fors, E. O., Jönsson, J. Å., and Swietlicki, E.: Source apportionment of carbonaceous aerosol in southern Sweden, Atmospheric Chemistry and Physics, 11, 11 387–11 400, https://doi.org/10.5194/acp-11-11387-2011, 2011.

Gensch, I., Kiendler-Scharr, A., and Rudolph, J.: Isotope ratio studies of atmospheric organic compounds: Principles, methods, applications and potential, International Journal of Mass Spectrometry, 365 - 366, 206 – 221, https://doi.org/http://dx.doi.org/10.1016/j.ijms.2014.02.004, 2014.

https://doi.org/10.5194/egusphere-2026-2593
Preprint. Discussion started: 23 June 2026

Gu, B., Zhang, L., Van Dingenen, R., Vieno, M., Van Grinsven, H. J. M., Zhang, X., Zhang, S., Chen, Y., Wang, S., Ren, C., Rao, S., Holland, M., Winiwarter, W., Chen, D., Xu, J., and Sutton, M. A.: Abating ammonia is more cost-effective than nitrogen oxides for mitigating $PM_{2.5}$ air pollution, Science, 374, 758–762, https://doi.org/10.1126/science.abf8623, 2021.

Guo, H., Otjes, R., Schlag, P., Kiendler-Scharr, A., Nenes, A., and Weber, R. J.: Effectiveness of ammonia reduction on control of fine particle nitrate, Atmospheric Chemistry and Physics, 18, 12 241–12 256, https://doi.org/10.5194/acp-18-12241-2018, 2018.

Holzinger, R., Goldstein, A. H., Hayes, P. L., Jimenez, J. L., and Timkovsky, J.: Chemical evolution of organic aerosol in Los Angeles during the CalNex 2010 study, Atmospheric Chemistry and Physics, 13, 10 125–10 141, https://doi.org/10.5194/acp-13-10125-2013, 2013.

Huang, L., Brook, J. R., Zhang, W., Li, S. M., Graham, L., Ernst, D., Chivulescu, A., and Lu, G.: Stable isotope measurements of carbon fractions (OC/EC) in airborne particulate: A new dimension for source characterization and apportionment, Atmospheric Environment, 40, 2690 – 2705, https://doi.org/https://doi.org/10.1016/j.atmosenv.2005.11.062, 2006.

Jayaraman, A., Lubin, D., Ramachandran, S., Ramanathan, V., Woodbridge, E., Collins, W. D., and Zalpuri, K. S.: Direct observations of aerosol radiative forcing over the tropical Indian Ocean during the January-February 1996 pre-INDOEX cruise, Journal of Geophysical Research: Atmospheres, 103, 13 827–13 836, https://doi.org/https://doi.org/10.1029/98JD00559, 1998.

Jonson, J. E., Fagerli, H., Scheuschner, T., and Tsyro, S.: Modelling changes in secondary inorganic aerosol formation and nitrogen deposition in Europe from 2005 to 2030, Atmospheric Chemistry and Physics, 22, 1311–1331, https://doi.org/10.5194/acp-22-1311-2022, 2022.

Kirillova, E. N., Andersson, A., Sheesley, R. J., Kruså, M., Praveen, P. S., Budhavant, K., Safai, P. D., Rao, P. S. P., and Gustafsson, Ö.: ^{13}C- and ^{14}C-based study of sources and atmospheric processing of water-soluble organic carbon (WSOC) in South Asian aerosols, Journal of Geophysical Research: Atmospheres, 118, 614–626, https://doi.org/10.1002/jgrd.50130, 2013.

Levin, I., Naegler, T., Kromer, B., Diehl, M., Francey, R., Gomez-Pelaez, A., Steele, P., Wagenbach, D., Weller, R., and Worthy, D.: Observations and modelling of the global distribution and long-term trend of atmospheric $^{14}CO_2$, Tellus B: Chemical and Physical Meteorology, 62, 26–46, https://doi.org/10.1111/j.1600-0889.2009.00446.x, 2010.

Martinsson, J., Andersson, A., Sporre, M. K., Friberg, J., Kristensson, A., Swietlicki, E., Olsson, P.-A., and Eriksson Stenström, K.: Evaluation of δ^{13}C in Carbonaceous Aerosol Source Apportionment at a Rural Measurement Site, Aerosol and Air Quality Research, 17, 2081 – 2094, https://doi.org/10.4209/aaqr.2016.09.0392, 2017.

Masalaite, A., Holzinger, R., Remeikis, V., Röckmann, T., and Dusek, U.: Characteristics, sources and evolution of fine aerosol (PM1) at urban, coastal and forest background sites in Lithuania, Atmospheric Environment, 148, 62 – 76, https://doi.org/https://doi.org/10.1016/j.atmosenv.2016.10.038, 2017.

Masalaite, A., Holzinger, R., Ceburnis, D., Remeikis, V., Ulevičius, V., Röckmann, T., and Dusek, U.: Sources and atmospheric processing of size segregated aerosol particles revealed by stable carbon isotope ratios and chemical speciation, Environmental Pollution, 240, 286–296, https://doi.org/https://doi.org/10.1016/j.envpol.2018.04.073, 2018.

Masalaite, A., Remeikis, V., Zenker, K., Westra, I., Meijer, H. A. J., and Dusek, U.: Seasonal changes of sources and volatility of carbonaceous aerosol at urban, coastal and forest sites in Eastern Europe (Lithuania), Atmospheric Environment, 225, 117 374, https://doi.org/https://doi.org/10.1016/j.atmosenv.2020.117374, 2020.

Masalaite, A., Holzinger, R., Plukis, A., Kairys, N., Meijer, H. A. J., and Dusek, U.: Chemical and isotopic characterization of carbonaceous aerosol particles from burning of different fuels, Atmospheric Research, 336, 108 895, https://doi.org/https://doi.org/10.1016/j.atmosres.2026.108895, 2026.

https://doi.org/10.5194/egusphere-2026-2593
Preprint. Discussion started: 23 June 2026

Matthias, V., Bewersdorff, I., Aulinger, A., and Quante, M.: The contribution of ship emissions to air pollution in the North Sea regions, Environmental Pollution, 158, 2241–2250, https://doi.org/https://doi.org/10.1016/j.envpol.2010.02.013, advances of air pollution science: from forest decline to multiple-stress effects on forest ecosystem services, 2010.

Mensah, A. A., Holzinger, R., Otjes, R., Trimborn, A., Mentel, T. F., ten Brink, H., Henzing, B., and Kiendler-Scharr, A.: Aerosol chemical composition at Cabauw, The Netherlands as observed in two intensive periods in May 2008 and March 2009, Atmospheric Chemistry and Physics, 12, 4723–4742, https://doi.org/10.5194/acp-12-4723-2012, 2012.

Meusinger, C., Dusek, U., King, S. M., Holzinger, R., Rosenørn, T., Sperlich, P., Julien, M., Remaud, G. S., Bilde, M., Röckmann, T., and Johnson, M. S.: Chemical and isotopic composition of secondary organic aerosol generated by α-pinene ozonolysis, Atmospheric Chemistry and Physics, 17, 6373–6391, https://doi.org/10.5194/acp-17-6373-2017, 2017.

Millero, F. J.: Chemical oceanography, CRC press, 1996.

Moroni, B., Cappelletti, D., Ferrero, L., Crocchianti, S., Busetto, M., Mazzola, M., Becagli, S., Traversi, R., and Udisti, R.: Local vs. long-range sources of aerosol particles upon Ny-Ålesund (Svalbard Islands): mineral chemistry and geochemical records, Rend. Fis. Acc. Lincei, 27 (Suppl 1), 115–127, https://doi.org/10.1007/s12210-016-0533-7, 2016.

Myhre, G., Shindell, D., Bréon, F.-M., Collins, W., Fuglestvedt, J., Huang, J., Koch, D., Lamarque, J.-F., Lee, D., Mendoza, B., Nakajima, T., Robock, A., Stephens, G., Takemura, T., and Zhang, H.: Anthropogenic and Natural Radiative Forcing, in: Climate Change 2013: The Physical Science Basis. Contribution of Working Group I to the Fifth Assessment Report of the Intergovernmental Panel on Climate Change, edited by Stocker, T., Qin, D., Plattner, G.-K., Tignor, M., Allen, S., Boschung, J., Nauels, A., Xia, Y., Bex, V., and Midgley, P., book section 8, p. 659–740, Cambridge University Press, Cambridge, United Kingdom and New York, NY, USA, ISBN ISBN 978-1-107-66182-0, https://doi.org/10.1017/CBO9781107415324.018, 2013.

Nel, A.: Air Pollution-Related Illness: Effects of Particles, Science, 308, 804–806, https://doi.org/10.1126/science.1108752, 2005.

Ni, H., Huang, R.-J., Yao, P., Cosijn, M. M., Kairys, N., Zhong, H., and Dusek, U.: Organic aerosol formation and aging processes in Beijing constrained by size-resolved measurements of radiocarbon and stable isotopic ^{13}C, Environment International, 158, 106 890, https://doi.org/https://doi.org/10.1016/j.envint.2021.106890, 2022.

Ni, H., Yao, P., Zhu, C., Qu, Y., Tian, J., Ma, Y., Yang, L., Zhong, H., Huang, R.-J., and Dusek, U.: Non-Fossil Origin Explains the Large Seasonal Variation of Highly Processed Organic Aerosol in the Northeastern Tibetan Plateau (3,200 m a.s.l.), Geophysical Research Letters, 50, e2023GL104 710, https://doi.org/https://doi.org/10.1029/2023GL104710, e2023GL104710 2023GL104710, 2023.

O'Leary, M. H.: Carbon Isotopes in Photosynthesis: Fractionation techniques may reveal new aspects of carbon dynamics in plants, BioScience, 38, 328–336, https://doi.org/10.2307/1310735, 1988.

Pope III, C. A. and Dockery, D. W.: Health Effects of Fine Particulate Air Pollution: Lines that Connect, Journal of the Air & Waste Management Association, 56, 709 – 742, https://doi.org/10.1080/10473289.2006.10464485, 2006.

Pöschl, U.: Atmospheric Aerosols: Composition, Transformation, Climate and Health Effects, Angewandte Chemie International Edition, 44, 7520–7540, https://doi.org/10.1002/anie.200501122, 2005.

Putaud, J.-P., Raes, F., Van Dingenen, R., Brüggemann, E., Facchini, M.-C., Decesari, S., Fuzzi, S., Gehrig, R., Hüglin, C., Laj, P., Lorbeer, G., Maenhaut, W., Mihalopoulos, N., Müller, K., Querol, X., Rodriguez, S., Schneider, J., Spindler, G., ten Brink, H., Tørseth, K., and Wiedensohler, A.: A European aerosol phenomenology—2: chemical characteristics of particulate matter at kerbside, urban, rural and background sites in Europe, Atmospheric Environment, 38, 2579–2595, https://doi.org/https://doi.org/10.1016/j.atmosenv.2004.01.041, 2004.

https://doi.org/10.5194/egusphere-2026-2593
Preprint. Discussion started: 23 June 2026

Reimer, P. J., Brown, T. A., and Reimer, R. W.: Discussion: Reporting and Calibration of post-bomb ^{14}C Data, Radiocarbon, 46, 1299–1304, 2004.

Rolph, G., Stein, A., and Stunder, B.: Real-time Environmental Applications and Display sYstem: READY, Environmental Modelling & Software, 95, 210–228, https://doi.org/https://doi.org/10.1016/j.envsoft.2017.06.025, 2017.

Schimmelmann, A., Qi, H., Coplen, T. B., Brand, W. A., Fong, J., Meier-Augenstein, W., Kemp, H. F., Toman, B., Ackermann, A., Assonov, S., Aerts-Bijma, A. T., Brejcha, R., Chikaraishi, Y., Darwish, T., Elsner, M., Gehre, M., Geilmann, H., Gröning, M., Hélie, J.-F., Herrero-Martín, S., Meijer, H. A. J., Sauer, P. E., Sessions, A. L., and Werner, R. A.: Organic Reference Materials for Hydrogen, Carbon, and Nitrogen Stable Isotope-Ratio Measurements: Caffeines, n-Alkanes, Fatty Acid Methyl Esters, Glycines, L-Valines, Polyethylenes, and Oils, Analytical Chemistry, 88, 4294–4302, https://doi.org/10.1021/acs.analchem.5b04392, 2016.

Schlag, P., Kiendler-Scharr, A., Blom, M. J., Canonaco, F., Henzing, J. S., Moerman, M., Prévôt, A. S. H., and Holzinger, R.: Aerosol source apportionment from 1-year measurements at the CESAR tower in Cabauw, the Netherlands, Atmospheric Chemistry and Physics, 16, 8831–8847, https://doi.org/10.5194/acp-16-8831-2016, 2016.

Schuur, E. A. G., Druffel, E., and Trumbore, S. E.: Radiocarbon and Climate Change - Mechanisms, Applications and Laboratory Techniques, Springer Cham, ISBN 978-3-319-25641-2, 2016.

Stein, A. F., Draxler, R. R., Rolph, G. D., Stunder, B. J. B., Cohen, M. D., and Ngan, F.: NOAA's HYSPLIT Atmospheric Transport and Dispersion Modeling System, Bulletin of the American Meteorological Society, 96, 2059 – 2077, https://doi.org/https://doi.org/10.1175/BAMS-D-14-00110.1, 2015.

Synal, H.-A., Stocker, M., and Suter, M.: MICADAS: A new compact radiocarbon AMS system, Nuclear Instruments and Methods in Physics Research Section B: Beam Interactions with Materials and Atoms, 259, 7 – 13, https://doi.org/https://doi.org/10.1016/j.nimb.2007.01.138, proceedings of the Tenth International Conference on Accelerator Mass Spectrometry, 2007.

Szidat, S., Jenk, T. M., Synal, H.-A., Kalberer, M., Wacker, L., Hajdas, I., Kasper-Giebl, A., and Baltensperger, U.: Contributions of fossil fuel, biomass-burning, and biogenic emissions to carbonaceous aerosols in Zurich as traced by ^{14}C, Journal of Geophysical Research: Atmospheres, 111, D07 206, https://doi.org/10.1029/2005JD006590, 2006.

Turšič, J., Podkrajšek, B., Grgić, I., Ctyroky, P., Berner, A., Dusek, U., and Hitzenberger, R.: Chemical composition and hygroscopic properties of size-segregated aerosol particles collected at the Adriatic coast of Slovenia, Chemosphere, 63, 1193–1202, https://doi.org/https://doi.org/10.1016/j.chemosphere.2005.08.040, 2006.

Vernooij, R., Dusek, U., Popa, M. E., Yao, P., Shaikat, A., Qiu, C., Winiger, P., van der Veen, C., Eames, T. C., Ribeiro, N., and van der Werf, G. R.: Stable carbon isotopic composition of biomass burning emissions – implications for estimating the contribution of C_3 and C_4 plants, Atmospheric Chemistry and Physics, 22, 2871–2890, https://doi.org/10.5194/acp-22-2871-2022, 2022.

Wacker, L., Christl, M., and Synal, H.-A.: Bats: A new tool for AMS data reduction, Nuclear Instruments and Methods in Physics Research Section B: Beam Interactions with Materials and Atoms, 268, 976–979, https://doi.org/https://doi.org/10.1016/j.nimb.2009.10.078, proceedings of the Eleventh International Conference on Accelerator Mass Spectrometry, 2010.

Warneck, P.: Chemistry of the Natural Atmosphere, Academic Press, 2nd edn., ISBN 9780080529066, 1999.

Weijers, E. P., Schaap, M., Nguyen, L., Matthijsen, J., Denier van der Gon, H. A. C., ten Brink, H. M., and Hoogerbrugge, R.: Anthropogenic and natural constituents in particulate matter in the Netherlands, Atmospheric Chemistry and Physics, 11, 2281–2294, https://doi.org/10.5194/acp-11-2281-2011, 2011.

https://doi.org/10.5194/egusphere-2026-2593
Preprint. Discussion started: 23 June 2026

Yao, P., Huang, R.-J., Ni, H., Kairys, N., Yang, L., Meijer, H. A., and Dusek, U.: ^{13}C signatures of aerosol organic and elemental carbon from major combustion sources in China compared to worldwide estimates, Science of The Total Environment, 810, 151 284, https://doi.org/https://doi.org/10.1016/j.scitotenv.2021.151284, 2022.

Yttri, K. E., Simpson, D., Nøjgaard, J. K., Kristensen, K., Genberg, J., Stenström, K., Swietlicki, E., Hillamo, R., Aurela, M., Bauer, H., Offenberg, J. H., Jaoui, M., Dye, C., Eckhardt, S., Burkhart, J. F., Stohl, A., and Glasius, M.: Source apportionment of the summer time carbonaceous aerosol at Nordic rural background sites, Atmospheric Chemistry and Physics, 11, 13 339–13 357, https://doi.org/10.5194/acp-11-13339-2011, 2011.

Zenker, K., Sirignano, C., Riccio, A., Chianese, E., Calfapietra, C., Prati, M. V., Masalaite, A., Remeikis, V., Mook, E., Meijer, H. A. J., and Dusek, U.: δ^{13}C signatures of organic aerosols: Measurement method evaluation and application in a source study, Journal of Aerosol Science, 145, 105 534, https://doi.org/https://doi.org/10.1016/j.jaerosci.2020.105534, 2020.

Zenker, K., Kasper-Giebl, A., Redl, P., and Dusek, U.: Dataset for "Measurement report: Size-resolved seasonal study of inorganic ions and isotopic carbon signatures of aerosol particles at the Wadden Sea", https://doi.org/10.5281/zenodo.19990975, 2026.

Zotter, P., El Haddad, I., Zhang, Y., Hayes, P. L., Zhang, X., Lin, Y.-H., Wacker, L., Schnelle-Kreis, J., Abbaszade, G., Zimmermann, R., Surratt, J. D., Weber, R., Jimenez, J. L., Szidat, S., Baltensperger, U., and Prévôt, A. S. H.: Diurnal cycle of fossil and nonfossil carbon using radiocarbon analyses during CalNex, Journal of Geophysical Research: Atmospheres, 119, 6818–6835, https://doi.org/10.1002/2013JD021114, 2014.